# Rotor Design Options for Improving XV-15 Whirl-Flutter Stability Margins

C. W. Acree, Jr., R. J. Peyran, and Wayne Johnson

The NASA STI Program Office . . . in Profile

Since its founding, NASA has been dedicated to the advancement of aeronautics and space science. The NASA Scientific and Technical Information (STI) Program Office plays a key part in helping NASA maintain this important role.

The NASA STI Program Office is operated by Langley Research Center, the Lead Center for NASA's scientific and technical information. The NASA STI Program Office provides access to the NASA STI Database, the largest collection of aeronautical and space science STI in the world. The Program Office is also NASA's institutional mechanism for disseminating the results of its research and development activities. These results are published by NASA in the NASA STI Report Series, which includes the following report types:

- TECHNICAL PUBLICATION. Reports of completed research or a major significant phase of research that present the results of NASA programs and include extensive data or theoretical analysis. Includes compilations of significant scientific and technical data and information deemed to be of continuing reference value. NASA's counterpart of peer-reviewed formal professional papers but has less stringent limitations on manuscript length and extent of graphic presentations.

- TECHNICAL MEMORANDUM. Scientific and technical findings that are preliminary or of specialized interest, e.g., quick release reports, working papers, and bibliographies that contain minimal annotation. Does not contain extensive analysis.

- CONTRACTOR REPORT. Scientific and technical findings by NASA-sponsored contractors and grantees.

- CONFERENCE PUBLICATION. Collected papers from scientific and technical conferences, symposia, seminars, or other meetings sponsored or cosponsored by NASA.

- SPECIAL PUBLICATION. Scientific, technical, or historical information from NASA programs, projects, and missions, often concerned with subjects having substantial public interest.

- TECHNICAL TRANSLATION. English-language translations of foreign scientific and technical material pertinent to NASA's mission.

Specialized services that complement the STI Program Office's diverse offerings include creating custom thesauri, building customized databases, organizing and publishing research results . . . even providing videos.

For more information about the NASA STI Program Office, see the following:

- Access the NASA STI Program Home Page at *http://www.sti.nasa.gov*

- E-mail your question via the Internet to help@sti.nasa.gov

- Fax your question to the NASA Access Help Desk at (301) 621-0134

- Telephone the NASA Access Help Desk at (301) 621-0390

- Write to:
  NASA Access Help Desk
  NASA Center for AeroSpace Information
  7121 Standard Drive
  Hanover, MD 21076-1320
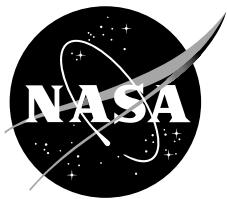
Rotor Design Options for Improving XV-15 Whirl-Flutter Stability Margins

C. W. Acree, Jr.
Ames Research Center, Moffett Field, California

R. J. Peyran
Aeroflightdynamics Directorate, U.S. Army Research, Development, and Engineering Command,
Ames Research Center, Moffett Field, California

Wayne Johnson
Ames Research Center, Moffett Field, California

Acknowledgments

Available from:

NASA Center for AeroSpace Information	National Technical Information Service
7121 Standard Drive	5285 Port Royal Road
Hanover, MD 21076-1320	Springfield, VA 22161
(301) 621-0390	(703) 487-4650

Table of Contents

Rotor Design Options for Improving XV-15 Whirl-Flutter Stability Margins

C. W. Acree, Jr.[1], R. J. Peyran[2], and Wayne Johnson[1]

[1]Ames Research Center

*[2]Aeroflightdynamics Directorate, U.S. Army Research, Development, and Engineering Command,
Ames Research Center*

Summary

Rotor design changes intended to improve tiltrotor whirl-flutter stability margins were analyzed. A baseline analytical model of the XV-15 was established, and then a thinner, composite wing was designed to be representative of a high-speed tiltrotor. Although the thinner wing had lower drag, it also had lower stiffness, reducing whirl-flutter stability. The rotor blade design was modified to increase the stability-speed margin for the thin-wing design. Small rearward offsets of the aerodynamic-center locus with respect to the blade elastic axis created large increases in the stability boundary. The effect was strongest for offsets at the outboard part of the blade, where an offset of the aerodynamic center by 10% of tip chord improved the stability margin by over 100 knots. Forward offsets of the blade center of gravity had similar but less pronounced effects. Equivalent results were seen for swept-tip blades: modest amounts of blade sweep starting at 80% radius created large increases in the stability boundary. Appropriate combinations of sweep and pitch stiffness completely eliminated whirl flutter within the speed range examined; alternatively, they allowed large increases in pitch-flap coupling (δ_3) for a given stability margin. A limited investigation of rotor loads in helicopter and airplane configuration showed only minor increases in loads.

Nomenclature

AC   blade section aerodynamic center, positive aft of EA

CG   blade chordwise center of gravity, positive forward of EA

C_T/σ thrust coefficient divided by solidity

EA   elastic axis

QC   blade quarter chord, positive aft of EA

r_{off} radial station for start of offset

R rotor radius

t/c wing thickness-to-chord ratio

Δ change in blade chordwise QC or CG position

δ_3 kinematic pitch-flap coupling ratio

μ advance ratio (flight speed divided by tip speed)

Ω rotor shaft speed

Introduction

Coupled wing/rotor whirl-mode aeroelastic instability is a major barrier to increasing tiltrotor speeds. Increased power, thrust, and rotor efficiency are of no avail unless the whirl-mode stability boundary can be improved. With current technology, very stiff, thick wings of limited aspect ratio are essential to meet the stability requirements, severely limiting cruise efficiency and maximum speed. Larger and more efficient tiltrotors will need longer and lighter wings, for which whirl-mode flutter is a serious design issue. Reference 1 gives a brief history of tiltrotor aeroelastic stability research and its application to tiltrotor design and flight test.

Numerous approaches to improving the whirl-mode airspeed boundary have been investigated, including tailored-stiffness wings (refs. 2–5), active stability augmentation (ref. 6), variable-geometry rotors (ref. 7), highly swept tips (ref. 8), and at one extreme, folding rotors (ref. 9). The research reported herein took an alternative approach of adjusting the chordwise positions of the rotor blade aerodynamic center (AC) and center of gravity (CG), effected by offsetting the airfoil quarter chord (QC) or structural mass with respect to the elastic axis (EA). The results implied the desirability of swept blades, hence the research was extended to include variations in blade sweep. The effects of control-system stiffness and pitch-flap coupling (δ_3) on stability were also studied in conjunction with sweep. The consequences for blade loads were briefly assessed. The XV-15 aircraft was the baseline.

This report discusses first the background to the research, which began with a small model constructed to facilitate rapid rotor design changes. A CAMRAD II analytical model is described, including a matrix of parametric variations of the rotor design. The design and analysis of a new, reduced-thickness wing are discussed. A summary

of results for all parametric variations is presented, followed by a few detailed examples. The effects on blade loads are also summarized.

This report presents a more comprehensive description of the research than previously available. Previously published material (refs. 10 and 11) is consolidated and expanded, and several appendices are added to document the research results in detail.

Background

The research began with a very simple, unpowered, table-top model of a wing and rotor (fig. 1), built of balsa wood and driven as a windmill by an ordinary box fan. The wing was a ladder-frame structure with no aerodynamic shell, and the rotor was a two-bladed, teetering design. This was the simplest design possible for testing whirl flutter. The 17-in diameter rotor had an adjustable weight on a rod extending ahead of the leading edge of each tip. Adjusting the chordwise weight position produced dramatic improvements in whirl-mode stability (ref. 12).
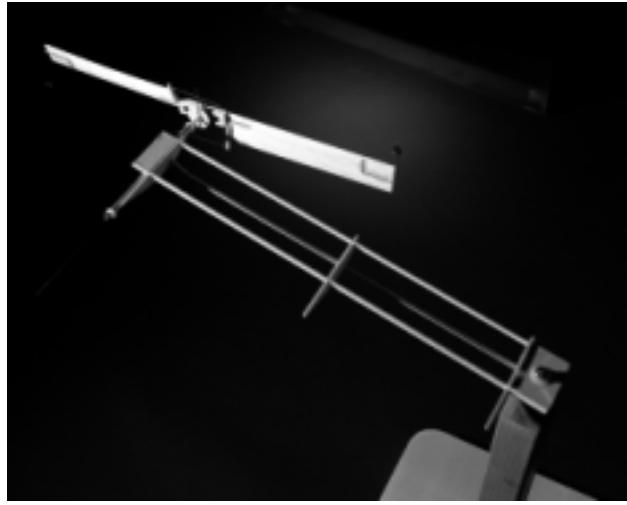

Figure 1. Table-top tiltrotor whirl-flutter model with tip weights.

Although hardly rigorous, the results were compelling and led immediately to analyses with CAMRAD II (ref. 10). A semispan analytical model of the XV-15 confirmed the results of the table-top model. The analytical model and its developments reported here have roots in earlier work reported in reference 13.

In classic flutter theory, the distance between the center of gravity and the aerodynamic center is a key parameter. This suggested that moving the aerodynamic center aft should have similar effects to moving the center of gravity forward. The CAMRAD II model was accordingly extended to examine an aerodynamic offset, but near the root of the blade instead of the tip. The aerodynamic offset improved whirl-mode stability, confirming the hypothesis. These favorable, preliminary results led directly to the more systematic efforts reported herein.

Analytical Model

The new CAMRAD II model was based closely on an existing model of the XV-15, chosen because it was well proven for stability analysis and thoroughly understood by the authors. See references 13 and 14 for correlations of CAMRAD predictions with measured stability and loads.

Figure 2 illustrates the XV-15 with pertinent dimensional data; the moderate aspect ratio of the thick wing is clearly evident. (Detailed specifications are given in reference 15; see also ref. 1.) The model used here was altered in several ways from the actual XV-15, including a different wing, a simplified drive-train model, and zero wing aerodynamic damping (except where noted). The changes are discussed further in the following paragraphs. The complete CAMRAD II model is listed in appendix A.

Airframe Model

Considerable effort was put into creating a thin, high-speed, graphite epoxy wing design that could be rigorously compared to the actual XV-15 wing. The new wing had the same planform as the XV-15 wing, but with a thickness-to-chord ratio (t/c) of 0.15, a value typical of current commuter aircraft, instead of 0.23. Airframe drag was arbitrarily reduced by 25% to simulate the improved aerodynamics expected from a thinner wing and other drag improvements typical of a high-speed design. The new wing was designed strictly for strength; no allowance was made for aeroelastic stability.

The design of the new wing model is documented in appendix B; table 1 lists key design parameters for the strength-designed thin wing, with values for the original aluminum wing and a flutter-designed thin wing. The last of these was designed with the same methods and material properties as the strength-designed thin wing, but was designed to the same flutter margins as the original aluminum wing. It remains to be seen whether the large predicted weight savings—over 45% for an 0.15-t/c wing—can be achieved in practice, but the possibility of even a much smaller weight reduction was a major motivation of the present research.
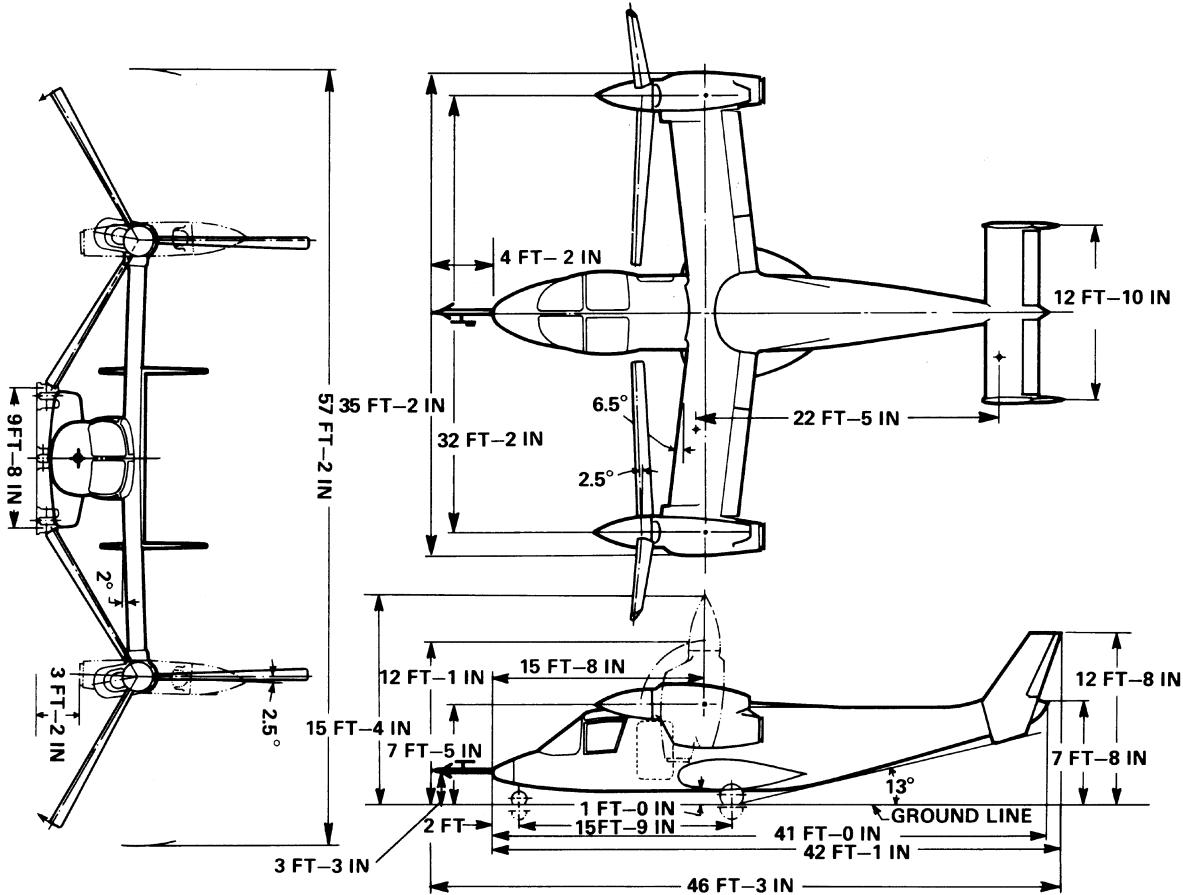
Figure 2. XV-15 tiltrotor aircraft geometry, with 0.23-t/c wing (ref. 15).

TABLE 1. WING STRUCTURAL COMPARISON

	XV-15 wing	Thin wing, strength designed	Thin wing, flutter designed
t/c	0.23	0.15	0.15
Weight, lb	946	579	1062
Material	Aluminum	Graphite epoxy	Graphite epoxy
Stiffness, lb-in^2:			
Beam bending	3.70E+09	1.98E+09	3.84E+09
Chord bending	1.12E+10	7.59E+09	1.16E+10
Torsion	2.80E+09	1.33E+09	2.80E+09

To calculate aeroelastic stability, CAMRAD II couples externally generated wing modes to internally generated rotor modes (ref. 16). Merely lowering the wing frequencies would not be adequate: the mode shapes must also be realistic for a thinner wing. The new wing was modeled in NASTRAN (ref. 17) to generate modal data for input into CAMRAD II.

The XV-15 airframe model evolved through three stages. Details are given in appendix C; a brief summary is given here. The original CAMRAD II model utilized wing mode shapes and frequencies generated by a detailed NASTRAN model. The second model used NASTRAN data from a much simpler "stick" model of the original, 0.23-t/c wing; this is denoted the "thick-wing" model. The third model, used in this study as a baseline reference, used NASTRAN data from a stick model of a 0.15-t/c wing; this is denoted the "thin-wing" model. The two NASTRAN stick models differed only in the parameters affected by wing thickness, thereby ensuring that comparisons between the thick and thin wings were not

3

affected by differences in NASTRAN modeling methods. The NASTRAN stick model is listed in appendix D.

The primary purpose of the thinner wing, at least as it applied to the present research, was to lower the whirl-mode airspeed stability boundary to better reveal the effects of parametric variations of the rotor. Because the rotor was not redesigned for higher speeds, the thin wing was of limited value for increasing cruise performance. Nevertheless, the new wing provided an adequate baseline, so the notional model was not further optimized.

Rotor Model

The baseline rotor used in the study is the original XV-15 steel-blade rotor, with a 2.5-deg precone titanium hub and -15-deg δ_3 (nominal). This is a stiff-in-plane rotor with a gimballed hub (ref. 15). The inboard aerodynamic sections start with a 17-in chord at 12% radius (R), linearly tapering to a 14-in chord at 25% R; the chord is constant from there to the tip (fig. 3). Total effective blade twist, from center of rotation to tip, is 45 deg over a 150-in R (ref. 18). The entire blade has 1-deg aft aerodynamic sweep, with the quarter-chord (QC) line intersecting the pitch axis at 75% R.

For all cases analyzed, the rotor was modeled in CAMRAD II (ref. 16) with a gimbal, two bending and one torsion mode per blade, and flexible pitch links. The left-right symmetry of the XV-15 was exploited by calculating symmetric and antisymmetric modes separately. A "rigid" drive-train model included the engine and gearbox inertias, but not drive-train flexibility or damping. (A full drive-train model would be needed for analysis of a production rotor, but its effects might not be consistent for all rotor design variations, so a rigid model was appropriate here.)

See appendix E for a discussion of the limitations of the CAMRAD II model used here.

Rotor Design Variations

The rotor parametric variations were distributed among four radial segments, numbered 1 to 4 from root to tip, as shown in figure 3. For simplicity, stepwise offsets were analyzed first. The aerodynamic center (AC) was offset chordwise aft in five increments of 5% of tip chord. (Local chord was not used, lest the inboard taper confound the results by creating an effective forward sweep along part of segment 1).

The shifts in AC were effected by shifting the airfoil aft with respect to the pitch axis, which in this model was the same as the blade elastic axis (EA). The airfoil was referenced to the QC. Figure 3 shows an example 10% QC aft offset at the tip segment.
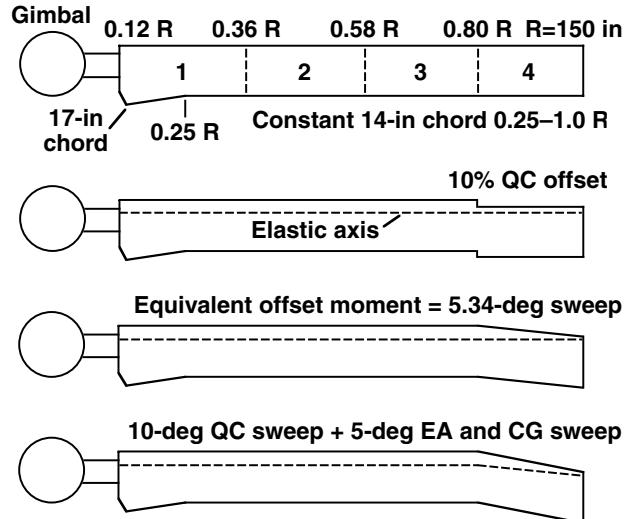
Figure 3. XV-15 rotor blade planform (45-deg twist and 1-deg baseline sweep not shown).

The center of gravity (CG) was offset forward in increments of 5% tip chord to match the magnitudes of the QC offsets. The maximum offset was, therefore, 25% chord, thus placing the CG at the leading edge. The two types of offset were analyzed separately. There were thus five discrete values of two parameters each, at four separate radial segments, making a matrix of 40 variations in addition to the baseline.

The stepped modifications were not intended to represent producible rotors, but to reveal the effects of the design parameters on stability. More realistic swept-tip blades were subsequently analyzed, as discussed later in this paper.

Aerodynamic and mass offsets are conceptually similar, in that they both increase the chordwise distance between the CG and AC. This is the classic means of increasing flutter stability of an isolated airfoil. Because of the highly coupled nature of whirl-mode instability, it also increases the stability of the entire rotor-wing dynamic system. However, the effects of aerodynamic offset are much stronger than those of mass offset, as will be shown.

Trim Criteria

Four different trim conditions were considered:

1. Level flight with unlimited power

2. Constant power (climb and dive to match power)

3. Zero power

4. Limited power (level flight up to maximum power; constant power thereafter)

4

The first is physically unrealistic, and the second is unrepresentative of actual flight operations. The third, zero power (windmill state), is a special case of constant power, and is a possible emergency flight condition (engine out). The fourth represents normal flight-test operations, wherein the aircraft is trimmed to level flight up to the power- or torque-limited airspeed, and then allowed to descend as necessary to achieve the desired airspeed at the torque limit.

Limited-power trim usually determines the whirl-mode stability boundary, but for some rotors, zero-power trim is the limiting condition, so both must be examined. For this research, limited-power trim always had a lower instability airspeed than zero power, although not by a large margin. Results for only the former are reported herein. Here a torque limit of 130,000 in-lb was used, reached at 275 knots with the thin wing.

The rotor was trimmed to 458 rpm (76% of hover design rpm) at sea-level standard conditions. This is the original design cruise rotor speed and is not representative of typical XV-15 operations; it was chosen because it is a nominal design point and highlights the effects of the parametric variations. The speed range was 150 to 400 knots true airspeed, with trim and stability calculated in 25-knot increments.

This report summarizes research performed over the course of two years. During that time, predictions were made with three different releases of CAMRAD II: 3.0, 3.1, and 3.2. Nearly all the results included here were generated by Release 3.1. To improve convergence, Release 3.2 introduced a new modeling option for a simulated gimballed hub, which gives better numerical behavior. For consistency, the simulated-gimbal option was not utilized for any predictions reported here.

Stability Predictions

If the cases discussed previously are added, there are 11 airspeeds for both trim criteria (zero power and limited power), applied to each of the 40 parametric variations, plus the thick- and thin-wing XV-15 models with the unmodified rotor, for a total of 924 cases. It is practical to present only a general overall summary and a few specific examples.

Baseline Checks

Figures 4 and 5 compare the CAMRAD II predictions for thick- and thin-wing XV-15 whirl modes, plotted as frequency and damping versus airspeed for each of the

wing modes. The intersections of the individual damping curves with the zero-damping axis define the stability boundaries for each mode; the overall whirl-flutter boundary is that of the least stable mode.

There are six wing modes to be examined: beamwise bending, chordwise bending, and torsion, each in symmetric (figs. 4(a) and 5(a)) and antisymmetric (figs. 4(b) and 5(b)) forms. The mode labels are somewhat arbitrary because the mode shapes rarely show pure bending, torsion, or chordwise deflections. This is especially true for the antisymmetric chord and torsion modes. Moreover, the blade collective lag mode couples strongly with the wing modes at high speeds. Figures 4 and 5 (and C4 and C5, in appendix C) merely summarize the modal responses; a presentation of all modal couplings is unnecessary for the purposes of this paper. The essential point is that all unstable modes are predicted with sufficient accuracy to reveal the effects of modifications to the rotor.

Figure 5 clearly shows that symmetric chord and antisymmetric beam are the limiting modes for both the thick- and thin-wing models. It also shows that reducing the wing thickness greatly reduces the symmetric chord, antisymmetric beam, and antisymmetric chord damping. The other modes are little affected, especially the symmetric beam mode. The stability boundary of the thin-wing model is barely 275 knots, a reduction of 60 knots below that of the original, thick wing. The key point is that the instability airspeed is greatly reduced without changing the basic nature of the limiting modes.

At 400 knots, the blade tip Mach number is 0.82, placing the tip airfoil section inside the transonic regime. The blade section lift-curve slope is decreasing at that point, improving stability. This effect can be clearly seen for symmetric chord (fig. 5(a)) and antisymmetric beam and torsion (fig. 5(b)).

Rigid-Rotor Stability

Figure 6 shows the stability of a rigid, gimballed XV-15 rotor with the thin wing. The rigid rotor was modeled simply by turning off all blade modes in the flutter analysis. This represents an idealized rotor that does not couple with the wing modes, except for the gimbal. The symmetric chord and antisymmetric beam modes are completely stable (as would be the symmetric beam mode if aerodynamic damping were included). These stability boundaries are not necessarily the minimum possible; nevertheless, they serve as useful goals against which to measure the effectiveness of the blade design variations discussed herein.
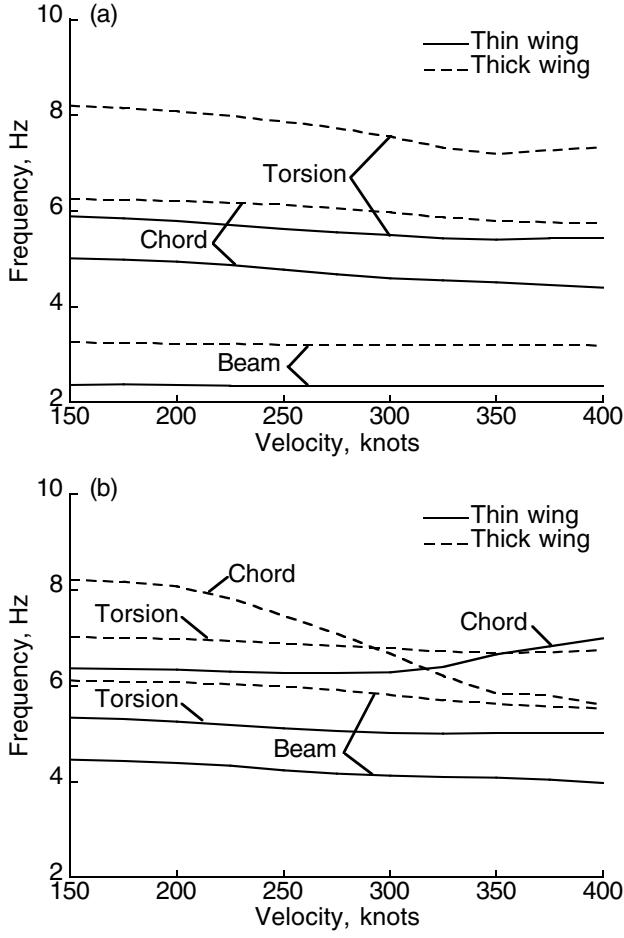
Figure 4. Whirl-mode frequency versus airspeed for the thick- and thin-wing models; (a) symmetric; (b) antisymmetric.
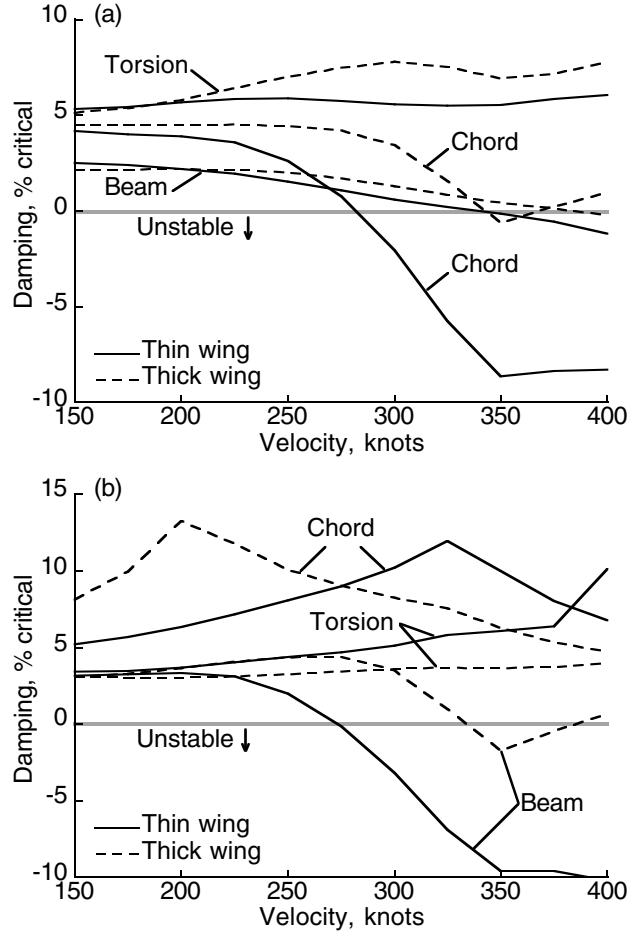
Figure 5. Whirl-mode damping versus airspeed for the thick- and thin-wing models; (a) symmetric; (b) antisymmetric.
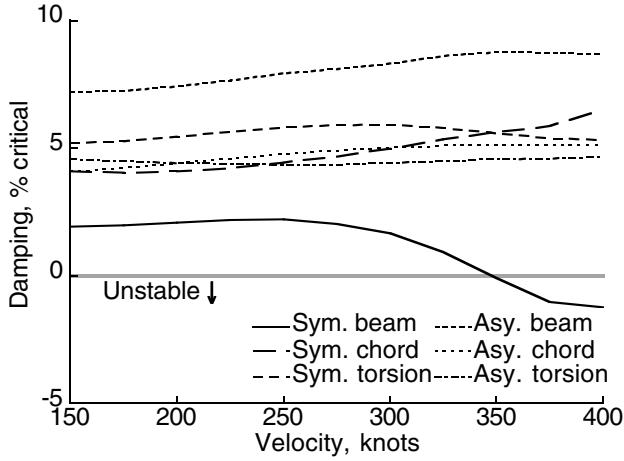
Figure 6. Whirl-mode damping versus airspeed for a rigid, gimballed rotor with the thin wing.

Summary of Parametric Variations for Stepped Offsets

Figures 7 and 8 summarize the changes to the overall stability boundary caused by the variations in blade QC and CG, modeled as stepped offsets. For the analyses discussed in this section, only one type of offset was applied at a time, and at only one radial segment at a time. The thin-wing airframe model was used in all cases.

The limiting airspeed was interpolated to the nearest 5 knots for each value of offset shown in figures 7 and 8. The lower limit of each plot is 275 knots, the stability boundary for the thin-wing model with the unmodified rotor. The stability boundary of the modified rotor never dropped below this speed. The upper limit of 400 knots was the maximum speed analyzed.

6

Eleven of the 40 QC and CG variations increased the instability airspeed by 60 knots or more, fully recovering the stability boundary of the original, thick-wing XV-15 model.

It is immediately apparent that QC offsets are much more effective than CG offsets: usually at least twice as much so (compare fig. 7 to fig. 8). Offsets at the tip are more effective than at the root for both types of offset.
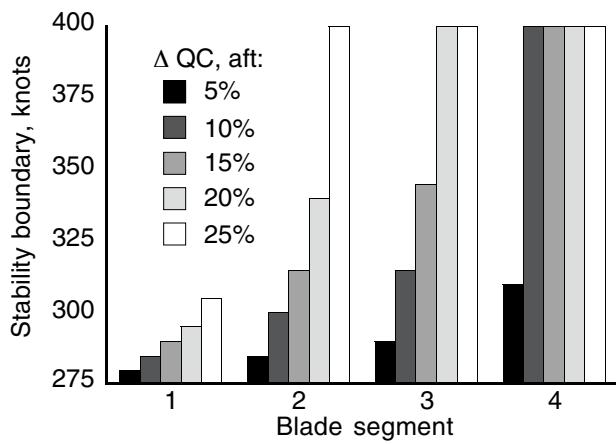
Figure 7. Whirl-mode stability boundaries for QC offsets, thin-wing model.
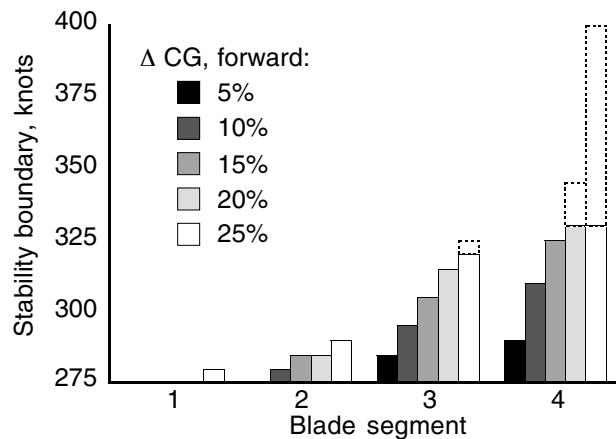
Figure 8. Whirl-mode stability boundaries for CG offsets, thin-wing model; dotted bars are antisymmetric mode limits.

For QC offsets, the limiting mode is usually antisymmetric beam, except for the 10% aft QC offset at segment 2, for which the symmetric beam mode determines the instability airspeed.

For CG offsets, the limiting mode is also usually the antisymmetric beam mode. The three exceptions are 25% forward CG offset at segments 3 and 4, and 20% forward CG offset at segment 4, for which the symmetric beam mode is the limiting mode.

The dotted lines in figure 8 represent the stability boundaries of the antisymmetric beam mode. Aerodynamic damping was neglected in the stability analyses. It would have increased the damping of the symmetric beam mode more than the other modes, so that all values would have shifted upwards, but by unequal amounts. The stability trends would then more closely follow the dotted bars in figure 8. The extended stability boundaries for segment 4 in figure 8 are generally similar to the boundaries of segment 2 in figure 7, revealing that both types of offset have similar effects on stability, aside from the greater overall effectiveness of QC offsets.

The effects of QC offsets were more pronounced than expected. The 400-knot limit of this study prevented a complete evaluation of the ultimate effectiveness of QC offsets at very high speeds, but exploitation of large stability improvements would require a reoptimized rotor. A 400-knot-class proprotor would have different airfoils, twist, and planform, and would, therefore, be expected to show different sensitivities to the parametric variations considered here.

The sensitivity of modal stability to the amount of QC and CG offset is revealed in more detail when the data are plotted for a single blade segment and fixed airspeed. Figures 9 and 10 present damping versus QC and CG offsets, respectively, for blade segment 4 at 350 knots. The outermost blade segment was chosen because the effects are most pronounced for that radial location. An airspeed of 350 knots was chosen because it is high enough to be strongly sensitive to both types of offset, yet not so high as to confound the results with transonic airfoil effects.

A comparison of figures 9 and 10 shows that any given amount of QC offset is much more effective than the same amount of CG offset, but only for offsets less than about 10% of tip chord. Increasing the QC offset has almost no effect beyond 15%, while CG offset is effective to the limit of the analysis, although it begins to be slightly less so at 25% offset.

For both types of offset, the wing modes most strongly affected are symmetric chord and antisymmetric beam. These are the critical modes because they are the least stable at zero offset. At a large enough value of either QC or CG offset, the damping of these two modes becomes greater than the damping of the symmetric beam mode, which is not strongly affected by either QC or CG offsets. However, this analysis included no wing aerodynamic damping, which would have raised the damping of the
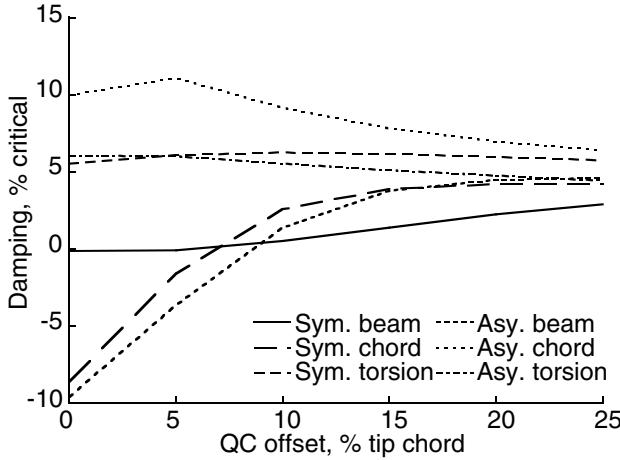
Figure 9. Variation of damping with QC offset for blade segment 4 at 350 knots.
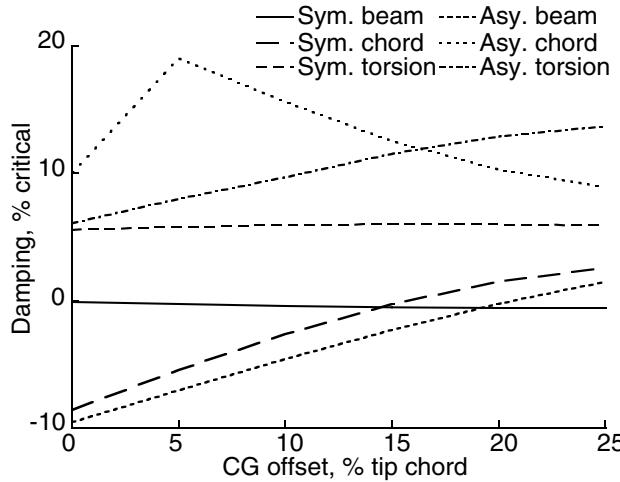
Figure 10. Variation of damping with CG offset for blade segment 4 at 350 knots.

symmetric beam mode more than any other mode. Therefore, definitive conclusions cannot be drawn from figures 9 or 10 concerning the optimum values of QC or CG offset.

Antisymmetric torsion is strongly influenced by CG offsets, but only slightly so by QC offsets. Antisymmetric chord is very sensitive to both offsets, and is the only mode that decreases significantly with either type of offset. Because the damping of both these modes is already high at zero offset, the variations shown here are of little consequence.

Antisymmetric chord damping exhibits the peculiar behavior of a large increase for a small amount of offset, then a decrease with increasing offset; the effect is

stronger for CG offsets (fig. 10) than for QC offsets (fig. 9). This is apparently caused by a strong interaction between wing and rotor modes, such that a small offset of either type significantly separates the modes, resulting in a large change in damping. When the modes are separated, further changes in offset have much less effect. The reader is reminded that mode labels are somewhat arbitrary because of these and other coupling effects. The rotor modes have higher damping than the whirl modes and accordingly are not shown in the figures.

The damping curves appear to be converging to a common value of about 5% critical damping, at least for QC offsets (fig. 9). This is roughly the same value as for a rigid, gimballed rotor (fig. 6). If the rotor did not dynamically couple with the wing at all, the wing (and nacelles) would still have a flutter boundary. A tentative conclusion is that at large enough values of QC offset, the rotor is fully stabilized and the flutter boundary is determined by the wing. Further increases to the offset would be expected to have little effect. However, symmetric beam damping is still improving with offset, but only slowly.

This speculation is only weakly supported by figure 10, but CG offsets would be expected to cause different modal couplings, hence different overall levels of stability.

Figure 9 helps to explain an anomaly noted previously for figure 7, wherein the limiting mode is the symmetric chord mode in all cases except one: as the QC offset becomes larger, symmetric chord damping increases faster than symmetric beam damping; eventually the chord damping exceeds the beam damping, but this effect is usually hidden by the whirl-flutter limits imposed by antisymmetric modes. A parallel effect is seen in figure 10 for CG offsets, as discussed previously for figure 8.

Detailed Examples

Two example rotors were chosen for closer study:

Rotor 1: 10% QC offset at blade segment 4

Rotor 2: 15% CG offset at blade segment 4

For reasons discussed previously, 400 knots was the limit of the analysis, hence a 125-knot increase of the stability boundary was the maximum considered. Even a 100-knot increase puts the rotor far beyond its design operating point and is more than enough to illustrate the relative effectiveness of QC and CG offsets. Therefore, 100 knots was chosen as the criteria for selecting the following examples.

From figure 7, the smallest QC offset giving a 100-knot benefit was chosen for example rotor 1. The maximum

increase for any CG variation is 55 knots (fig. 8). The minimum CG offset needed to achieve this improvement was chosen for example rotor 2. Stability predictions for example rotors 1 and 2 are plotted in figures 11 and 12, respectively; all predictions are based on the thin-wing airframe model.

Figure 11 shows the effects of 10% QC offset at blade segment 4 (example rotor 1); the damping values for this rotor are plotted against those for the reference rotor. The symmetric chord (fig. 11(a)) and antisymmetric beam (fig. 11(b)) modes are the most dramatically affected. These are the two modes with the lowest stability speeds for the reference rotor, so increasing their damping would have the largest effect on overall stability. Only the symmetric beam mode becomes unstable within the limit

of the analysis. Had aerodynamic damping been included in the analysis, all modes would have probably remained stable to 400 knots.

Figure 12 shows the effects of 15% CG offset at blade segment 4 (example rotor 2). Again, the symmetric chord (fig. 12(a)) and antisymmetric beam (fig. 12(b)) modes are the most changed. The symmetric beam damping is almost unchanged, but it is only slightly less stable than symmetric chord (fig. 12(a)). With aerodynamic damping, symmetric beam would probably have been more stable than symmetric chord at high airspeeds. Antisymmetric torsion is also strongly affected (fig. 12(b)), but because it is already heavily damped, the improvement is of comparatively little significance.
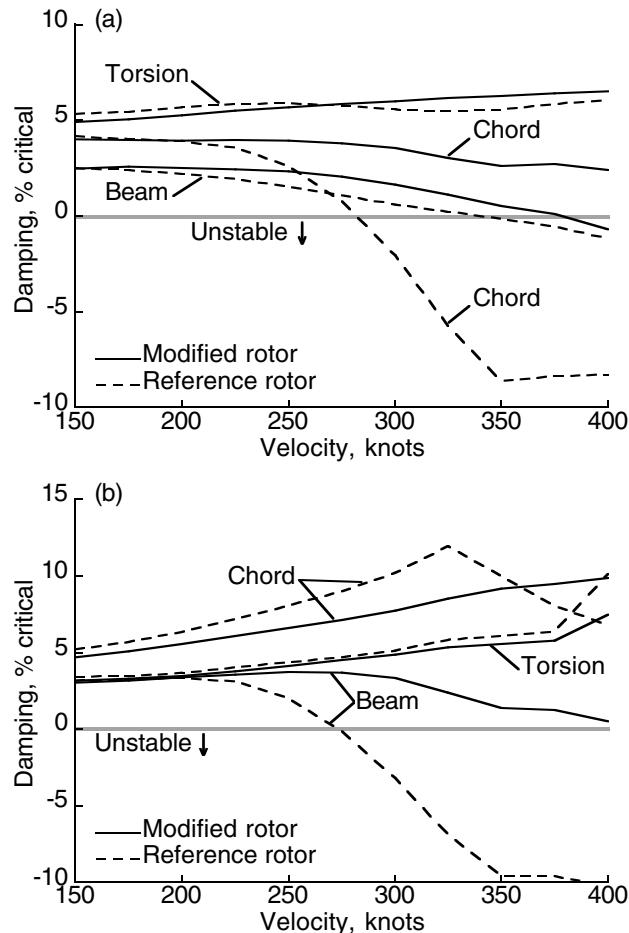
Figure 11. Whirl-mode damping versus airspeed for 10% QC offset at blade segment 4; (a) symmetric; (b) antisymmetric.
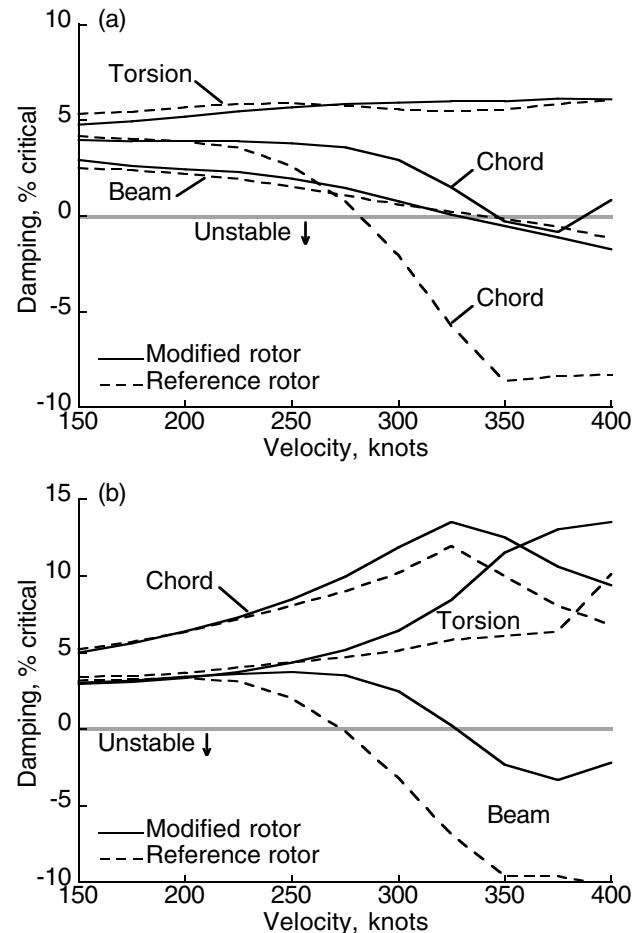
Figure 12. Whirl-mode damping versus airspeed for 15% CG offset at blade segment 4; (a) symmetric; (b) antisymmetric.

In both examples, the modifications make the greatest improvements to the lowest-damped modes—symmetric chord and antisymmetric beam—with no significant reduction in the damping of the other modes. Note that because of the gradual slope of symmetric beam damping, a small change to its damping would cause a large change in its stability speed. Inclusion of aerodynamic damping would, therefore, be expected to significantly increase the flutter boundary of the symmetric beam mode.

Radial Extent

Figure 13 addresses the question, is it better to have a small offset distributed over a large radial extent of the blade, or a large offset distributed over a small radius? For this analysis, the offset always extended from the starting radius to the tip. As the starting point r_{off} was varied, the amount of offset, ΔQC or ΔCG, was adjusted to maintain an equal offset moment, which is simply the amount of offset multiplied by the distance to the blade tip; e.g.,

$$\Delta QC \times (R - r_{off}) = \text{Constant}$$

For both QC and CG offsets, the reference values were 10% offset starting at 0.8 R (blade segment 4). Damping was calculated at 350 knots for the thin wing, consistent with figures 9 and 10. For clarity, only the least stable modes—symmetric chord and antisymmetric beam—are shown.
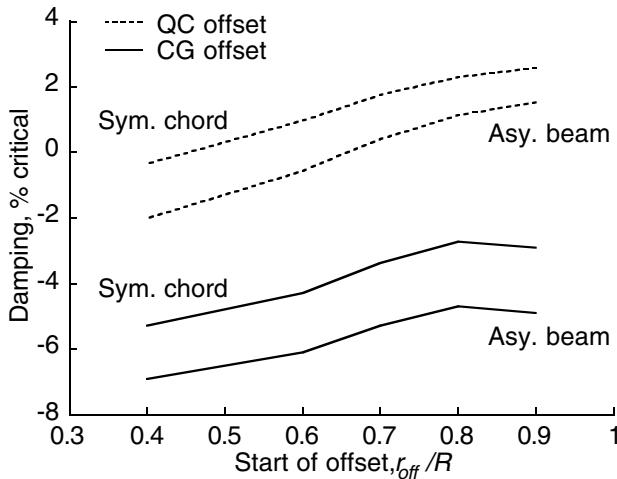
Figure 13. Variation of damping with radial extent of offset for constant offset moment at 350 knots; reference is 10% offset at blade segment 4.

The results suggest that it is better to concentrate the offset near the tip, consistent with figures 7 and 8. For CG offsets, there is a maximum improvement near 0.8 R, and

for QC offsets, the effectiveness of moving the offset further outboard appears to diminish beyond 0.8 R. However, this analysis does not constitute a true optimization because the possibility of numerical effects cannot be excluded. As the radial extent of offset decreases, there are necessarily fewer radial stations at which blade properties are specified in the CAMRAD II model. A very small radial extent incurs the risk of numerical artifacts, especially for stepped offsets, and can be nullified by tip-loss effects. For this reason, the analysis was not extended to offset starting points outboard of 0.9 R. Nevertheless, the results presented here show that 0.8 R was a reasonable point at which to start the offsets.

Combined Offsets

Because of complex modal couplings plus the nonlinear sensitivity of damping to offset (figs. 9 and 10), it cannot be assumed that QC and CG offsets are compatible. Figures 14 and 15 illustrate combined offsets, where one type of offset is held at a fixed value while the other is varied. As in figures 9 and 10, offsets were applied to the outermost blade segment and stability was calculated at 350 knots. Only the least stable modes are shown.

Figure 14 shows the effects of varying QC offset while the CG offset is held at 15% chord (the same value as in example rotor 2, defined previously). For comparison, damping curves for QC variations with zero CG offset are also shown. With a 15% CG offset, the damping is significantly increased for low values of QC offset, and the nonlinear sensitivity of damping to changes in offset is still evident, as is convergence to a value just under 5% damping. However, the overall sensitivity to QC offset is much reduced.

Figure 15 shows the effects of varying CG offset while the QC offset is held at 10% chord (the same value as in example rotor 1). Damping curves for CG variations with zero QC offset are also shown. Again, the damping is increased much more at low values of CG offset than at high values. The overall damping is consistently increased for combined offsets and appears to be converging toward a value slightly under 5%.

The common result is that QC and CG offsets can be combined for an increase in damping, but their effects do not add linearly. Fortunately, most of the reduction in sensitivity to offset occurs after the system is stable, so the asymptotic behavior presents no problems.

Swept-Tip Blades

Figures 13, 14, and 15 together imply that swept tips would increase whirl-mode stability. Aft sweep would move the CG in an unfavorable direction, but the greater

sensitivity of damping to QC offset would cause a net increase in stability. Sweep would also maximize the amount of offset at the tip for a slight improvement over a stepped offset, and would make for more practical blade construction. Note that blade sweep is derived from different considerations than those that apply to classic swept wings.
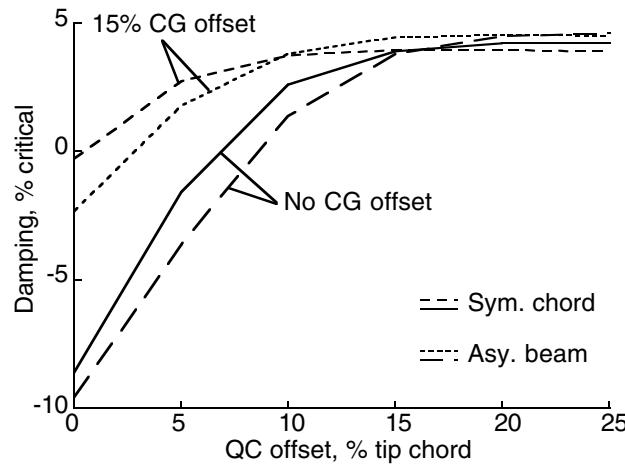
Figure 14. Variation of damping with QC offset while CG offset is held fixed for blade segment 4 at 350 knots.
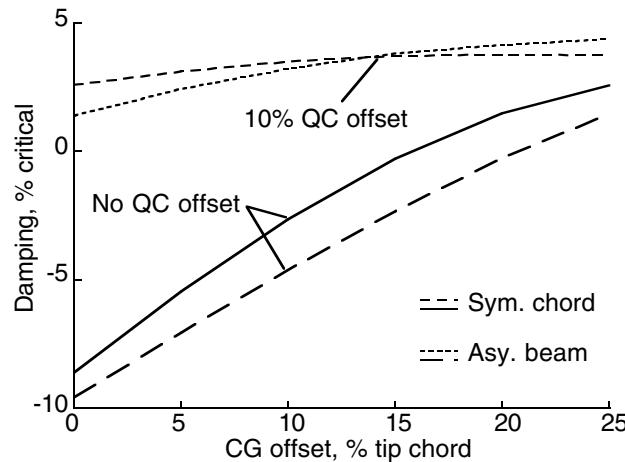
Figure 15. Variation of damping with CG offset while QC offset is held fixed for blade segment 4 at 350 knots.

Figure 3 shows two blades with swept tips. The first has 5.34 deg of sweep over the outer 20% of blade radius, giving the same offset moment as a 10%-chord offset. That is, the product of the local offset and the incremental chord, integrated over the outermost blade segment, is the same for both a 10% stepped offset and a 5.34-deg swept

blade. The second swept blade has 10 deg of sweep over the outer 20% radius, the maximum analyzed in this study.

For the stability analyses discussed herein, sweep was modeled by sweeping the EA and QC locus, either together or separately, as explained in the following paragraphs. In CAMRAD II, structural and aerodynamic parameters are referenced to the EA and QC locus, respectively, so they are automatically swept with the EA and QC (ref. 16). Sweep was always initiated at $0.8\,R$ (blade segment 4 in fig. 2); the outer 20% of the blade was, in effect, rotated aft by the amount of sweep. Damping was calculated at 2-deg increments of sweep.

Figures 16 and 17 show the variation in damping with sweep for blades with aerodynamic sweep only and with equal aerodynamic and structural sweep. The first is not a practical blade; indeed, at high values of sweep, it cannot physically exist because the CG and EA are both ahead of the leading edge at the tip. Nevertheless, the purely theoretical results are instructive because they clearly show that sweep is equivalent to a stepped offset: the damping curves in figures 9 and 16 are very similar.

Figure 17 shows the predicted damping for a blade with a fully swept tip. This blade is far more practical than that of figure 16, but the aft sweep of the CG greatly reduces the increase in damping. There is still a net improvement to stability.

Figure 18 shows results for a blade with its EA and CG swept one-half as much as the QC. Although unconventional, such a blade would be feasible as long as the sweep did not start too far inboard. The damping of the least stable modes is much improved over that of figure 17; at high values of sweep, it is almost as good as that for blades with only aerodynamic sweep (fig. 16).

It should be emphasized that all analyses reported here are based on the original XV-15 steel blades, for which the manufacturability of any modification is highly problematical. A swept tip would be more practical to implement with a modern, composite structure. Because the particular designs considered here have no likelihood of being constructed, and because the results shown in figure 17 are more than adequate to illustrate the benefits of the concept, no further optimization of the blade design was undertaken. A blade with 10-deg aerodynamic and 5-deg structural sweep was chosen for further study, as discussed in the following sections.
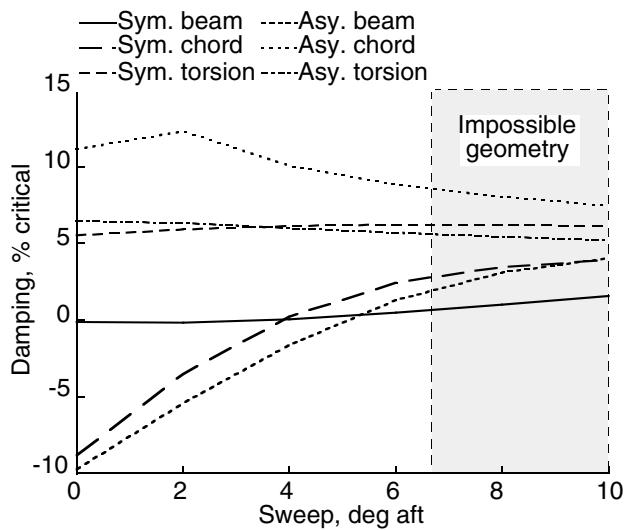
Figure 16. Variation of damping with QC sweep at 350 knots; the structure is not swept.
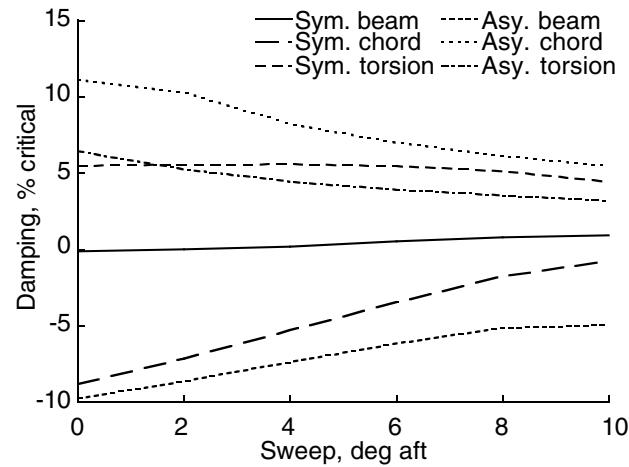
Figure 17. Variation of damping with full sweep at 350 knots.
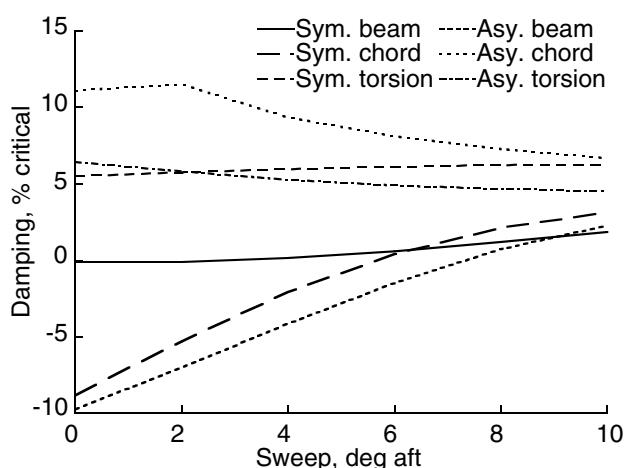
Figure 18. Variation of damping with sweep at 350 knots; the structural sweep is one-half the aerodynamic sweep.

Control-System Stiffness

The stiffness of the control system has a strong effect on aeroelastic stability, as shown in figure 19 for the baseline rotor. The baseline pitch stiffness seen by the blade is multiplied by a stiffness factor, against which damping is plotted. (The baseline value is 22,400 ft-lb/rad.) CAMRAD II allows the pitch links to be analytically locked, yielding the equivalent of infinite stiffness. Infinite stiffness yields damping values negligibly different from a stiffness factor of 100, so the stiffness scale in figure 19 is truncated at that value. For clarity, the scale is logarithmic to expand the damping curves at low values of stiffness while simultaneously revealing the asymptotic behavior at high values. Damping is shown at 350 knots for the thin wing, consistent with figures 13–18.
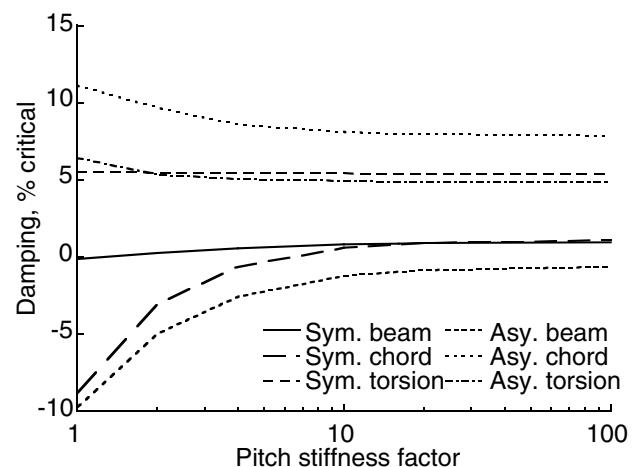
Figure 19. Variation in damping with pitch stiffness factor for the baseline XV-15 rotor at 350 knots.

Figure 19 shows that about half of the maximum increase in damping is obtained with a pitch stiffness factor of two, and further increases in stiffness yield progressively diminishing increases in damping. A stiffness factor of two was used in selected analyses that follow. The V-22 has roughly three times the scaled pitch stiffness of the XV-15, so a factor of two is reasonable and no further optimization was undertaken.

Figure 20 shows the results of combining tip sweep with an increased-stiffness control system. As in figure 18, the aerodynamic sweep is twice the structural sweep. The asymptotic behavior of damping with sweep reduces the effect of increased control stiffness (compare fig. 20 with fig. 18); at high enough values of sweep, the increase in damping is negligible. However, the system becomes stable at a lower value of sweep: about 7 deg instead of 9 deg, a useful improvement.
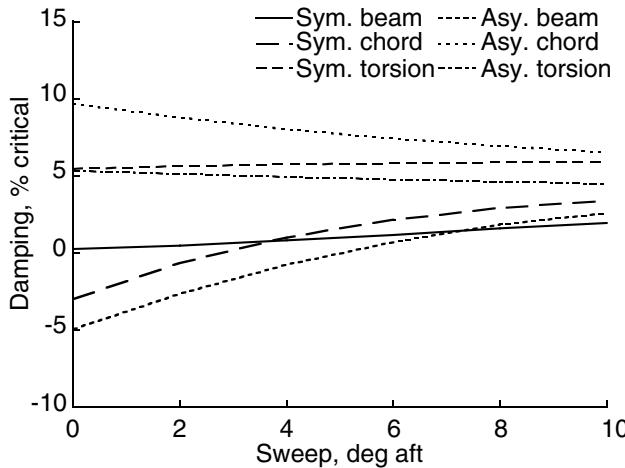
Figure 20. Variation of damping with sweep at twice the baseline pitch stiffness at 350 knots; the structural sweep is one-half the QC sweep.
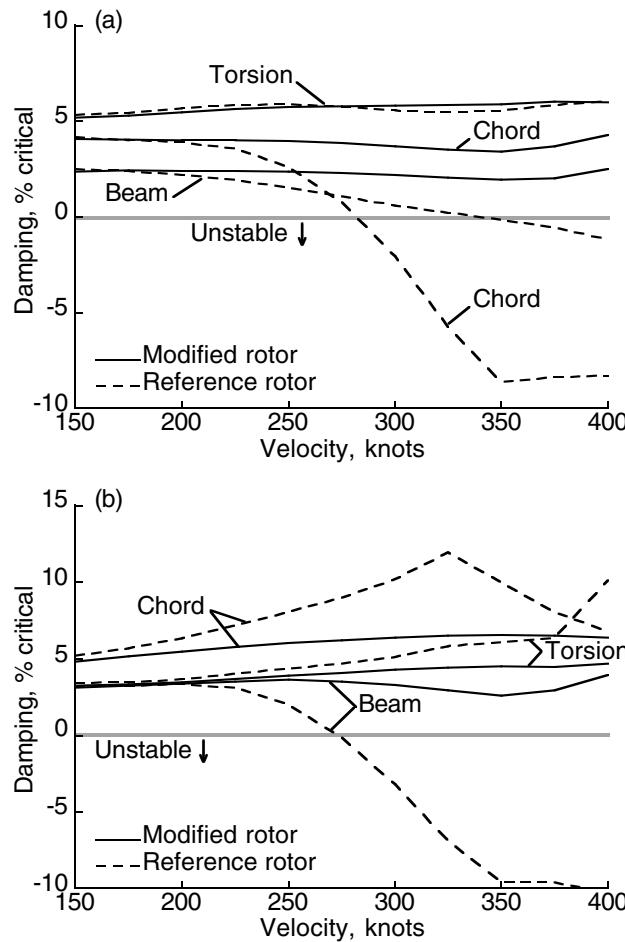
Figure 21. Whirl-mode damping versus airspeed at twice the baseline pitch stiffness, 10-deg QC sweep, and 5-deg structural sweep; (a) symmetric; (b) antisymmetric.

The trends of damping with airspeed are shown in figure 21 for combined tip sweep and increased control-system

stiffness. The rotor is the same as that analyzed for figure 20 at maximum sweep. For ease of comparison, the format is the same as that for figures 4, 5, 6, 11, and 12; the "reference rotor" lines in figure 21 correspond to the "thin wing" lines in figures 4 and 5. Note that all whirl modes, including the symmetric beam mode, show little variation in damping with airspeed; the wing/rotor system is now completely stable.

Variations in δ_3

So far in this paper, blade modifications have been studied for the purpose of extending the XV-15 whirl-flutter boundary for a thin wing. Improvements to whirl-mode damping can be exploited for other purposes, an example of which is discussed in the following paragraphs.

δ_3 is the kinematic coupling between blade flapping and pitch (ref. 19). As defined herein, positive δ_3 causes nose-down pitching for upward blade flapping. This counterintuitively *decreases* dynamic stability for some blade modes, typically lag modes. The realization that negative δ_3 is stabilizing was a major conceptual breakthrough necessary for the successful development of the XV-15 (ref. 20).

Because the effective flapping hinge is at the center of rotation of a gimballed rotor, a literal skewed hinge is not possible on the XV-15, so offset pitch horns must be used. The XV-15 has trailing pitch horns, as shown in figure 22. Furthermore, it is extremely difficult to arrange the pitch horns to achieve small values of δ_3 without mechanical interference, especially for rotors with four or more blades. As the magnitude of δ_3 increases, whirl-mode stability rapidly decreases.
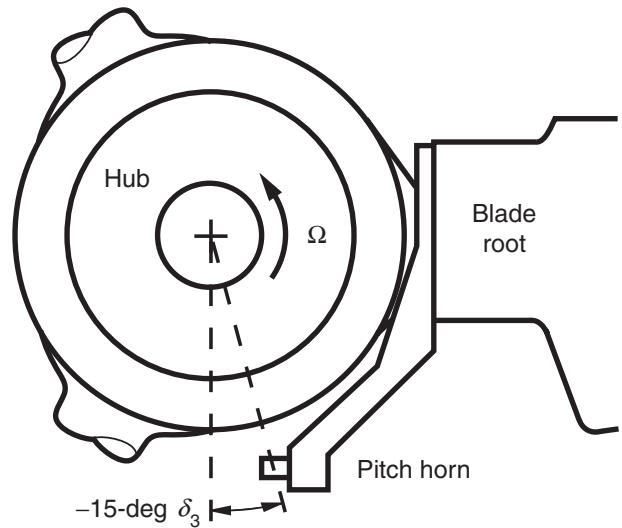
Figure 22. XV-15 hub and trailing pitch horn.

These effects constrain practical design values of δ_3 to a narrow range of negative values. The XV-15 design value of δ_3 is –15 deg (ref. 15), realized by a trailing, offset pitch horn. All values of δ_3 discussed herein are nominal values; the actual value varies slightly as the pitch horn moves with changing collective and cyclic control inputs.

Figure 23 shows the variation of damping with δ_3 for the baseline XV-15 (thick wing) and unmodified rotor. The airspeed is 300 knots, the design maximum. Because the original wing design was used, and because most analyses of δ_3 were done at the same airspeed, aerodynamic damping was included in the model. The damping predicted by CAMRAD II becomes negative between –20- and –25-deg δ_3. The actual aircraft must have a margin of stability, so the design magnitude of δ_3 must be less than the zero-damping value. Figure 23 indicates that –15 deg is a reasonable value, consistent with XV-15 experience.
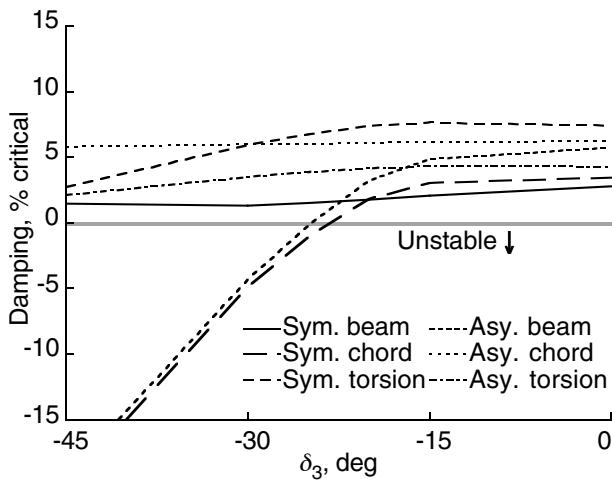
Figure 23. Variation of damping with δ_3 for the baseline XV-15 and unmodified rotor at 300 knots.

Damping of the unstable modes varies almost linearly with δ_3 until it approaches the limiting, stable value consistent with figures 14–20 (although maximum antisymmetric beam damping is a bit higher). Damping for positive δ_3 is not shown because certain rotor modes, principally blade lag modes coupled with wing modes, are always unstable.

Figure 24 shows results for a control-system stiffness factor of two. The value of δ_3 for zero damping is extended to almost –35 deg.

Figure 25 shows results for a rotor with 10-deg aerodynamic sweep and 5-deg structural sweep over the outmost 20% blade radius. This is the most extreme

sweep plotted in figures 16–18 and is the most effective of the practical blade designs examined here. The airspeed is 300 knots, the same as for figures 23 and 24. The δ_3 value for neutral stability is extended to almost –45 deg. The two least stable modes at –45-deg δ_3 become the most stable modes near –35 deg, then they asymptotically approach the limiting values seen in the previous plots.
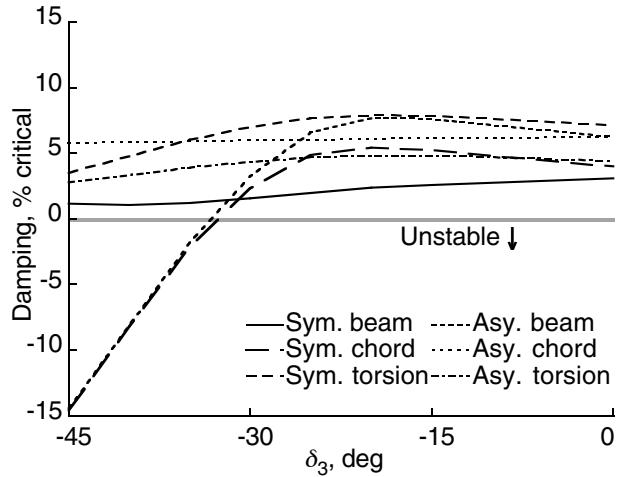
Figure 24. Variation of damping with δ_3 for the baseline XV-15 with twice the baseline pitch stiffness at 300 knots.
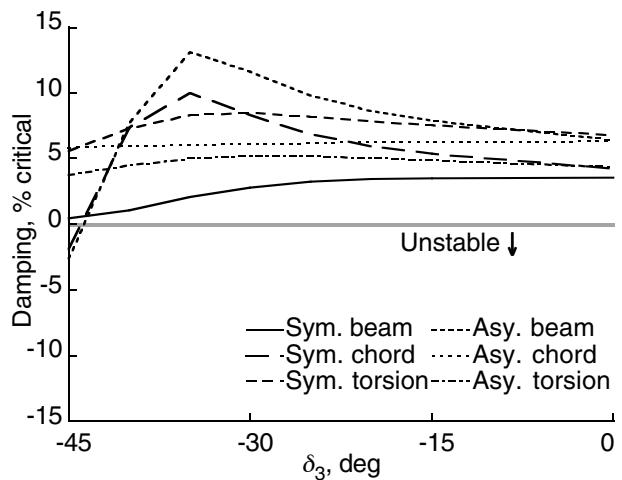
Figure 25. Variation of damping with δ_3 for the baseline XV-15 with 10-deg QC sweep and 5-deg structural sweep at 300 knots.

The final stability analysis combined the increased control-system stiffness of figure 24 with the swept tip of figure 25; the results are shown in figure 26. Whirl-mode damping is positive for $\delta_3 = $ –45 deg. This value of δ_3 was the maximum studied because no further increase is

necessary for a four-bladed rotor, and because the incremental improvement caused by the increased control-system stiffness is very minor compared to that shown in figure 25.
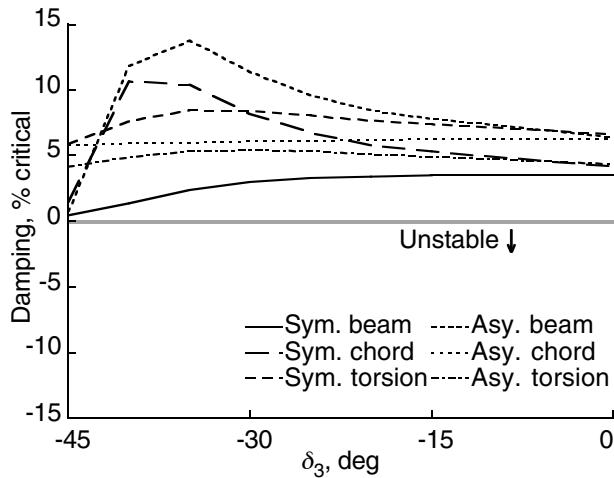
Figure 26. Variation of damping with δ_3 for the baseline XV-15 with twice the baseline pitch stiffness, 10-deg QC sweep, and 5-deg structural sweep at 300 knots.

Loads Implications

Two rotor designs were analyzed further to estimate their effects on rotor loads. Both designs used the most effective rotor developed during this study, with 10-deg aerodynamic sweep, 5-deg structural sweep, and twice the baseline control stiffness. Design A had the 0.15-t/c wing with -15-deg δ_3, and design B had the 0.23-t/c wing with -45-deg δ_3. Two flight conditions were analyzed:

1. Airplane mode at 250 knots, 458 rpm ($\mu = 0.70$), rotor $C_T/\sigma = 0.027$.

2. Helicopter mode (nacelle angle = 75 deg) at 80 knots, 565 rpm ($\mu = 0.18$), rotor $C_T/\sigma = 0.088$.

The airplane-mode condition was chosen to ensure that the loads were calculated within the thin-wing stability boundary (fig. 5) to provide a valid baseline reference.

Predictions of mean and one-half peak-to-peak oscillatory loads are plotted in figures 27 and 28. The figures include flap and lag bending moments at $0.35\,R$ and pitch link force, all normalized to the reference (unmodified) rotor for the appropriate wing. Helicopter-mode loads are normalized to the helicopter reference, and airplane-mode loads are normalized to the airplane reference. Mean and oscillatory loads are plotted separately. The results for the example designs are plotted adjacent to each other for comparison, and airplane-mode results are plotted

adjacent to helicopter-mode results for each type of load (lag, flap, and pitch-link loads). (See ref. 10 for loads predictions for stepped-offset blades.)

All loads analyses included 6 harmonics of blade motion and 12 blade modes. In airplane mode, the analysis included wing/body interference velocities at the rotor. Uniform inflow was assumed because the differences caused by blade dynamics were of interest, for which momentum theory was adequate, especially in airplane mode. Development of a full wake model for helicopter flight was not justified at this stage of the research, which focused on flutter, not loads. The objective of the loads analysis was to check for large adverse load variations.
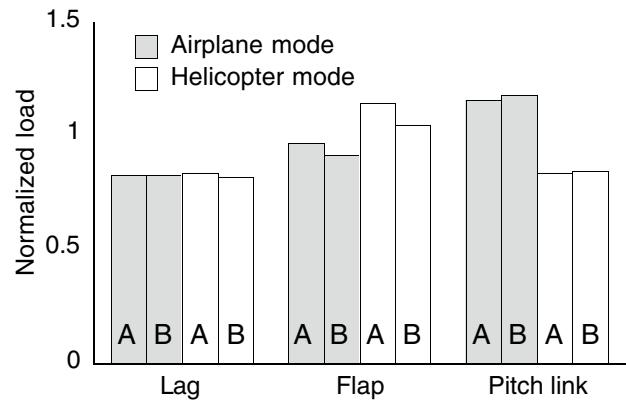
Figure 27. Mean rotor loads, normalized to the baseline rotor, for designs A and B.
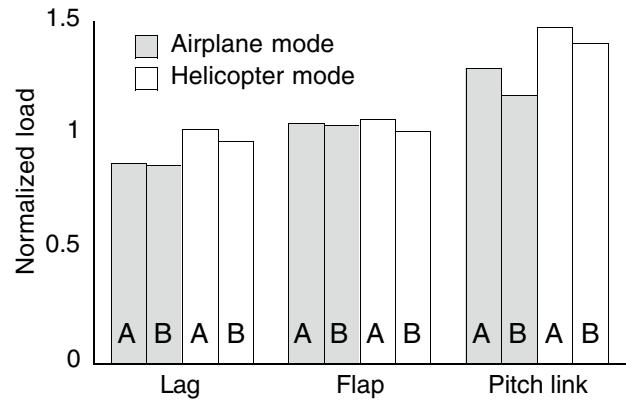
Figure 28. Oscillatory rotor loads, normalized to the baseline rotor, for designs A and B.

Examination of figure 27 shows that neither of the design variations has severely adverse effects on mean loads in airplane mode. Mean flap-bending loads are almost always reduced compared to the baseline rotor.

15

In figure 28, lag- and flap-bending oscillatory loads are little affected, but pitch-link loads are significantly increased in airplane mode for both designs. However, the normalization against loads in the same flight condition exaggerates the effect. In fact, oscillatory loads are lower in airplane mode than in helicopter mode.

Although not a comprehensive loads survey, these results are enough to show that loads increases should be acceptable. No attempt was made to adjust balance weights or otherwise tune the rotor for loads, so it should be possible to reduce the loads below those shown here. The key result is that there exist combinations of parameters that give large increases in the whirl-mode stability boundary without excessive increases in loads.

Conclusions and Recommendations

The XV-15 rotor was analyzed with CAMRAD II to examine the effects on whirl-mode aeroelastic stability of chordwise offsets of the rotor blade QC and CG relative to the EA. The XV-15 model was modified to have a thinner wing (0.15 t/c) to better reveal the effects of the modifications. Small rearward offsets of the QC created large increases in the stability boundary, in some cases by over 100 knots. The effect grew progressively stronger as the QC and CG offsets were shifted radially outboard. Forward offsets of the blade CG had similar effects, but the maximum improvement seen was limited to 55 knots. For the range of offsets analyzed, CG offsets had a more linear effect on stability than QC offsets. Swept-tip blades showed stability improvements similar to stepped-offset designs.

Proper choice of parametric variations can avoid excessive increases in rotor loads. Limited-power trim proved slightly less stable than windmill-state trim.

These results can be applied to tiltrotors in several ways, most obviously to reduce the wing thickness for improved cruise performance while retaining adequate whirl-mode stability margins. In the present study, the wing t/c was reduced from 0.23 to 0.15 without decreasing the whirl-mode boundary. Thickness could in principle be retained while reducing weight or increasing aspect ratio, as appropriate for the performance goals of a particular design.

Offsets of the blade AC and CG, or the equivalent sweep, should be utilized as primary design variables because of their powerful effects on whirl-mode stability.

The improvements to whirl-mode stability could also be used to expand the range of δ_3. A sufficiently large increase in δ_3 would permit designing four-bladed rotors with otherwise conventional gimballed hubs.

The present study analyzed a broad range of large offsets. Follow-on research should examine smaller increments of the key parameters, and should focus on the outboard blade segments, where the effect was largest. This would better define optimum values and sensitivities for more realistic design values. It would also be appropriate to examine the effects for a rotor explicitly designed for very high speeds, with re-optimized twist, airfoil sections, taper, etc. The analysis could be usefully extended to more radical blade concepts, such as inverse-taper and external mass booms. In addition, the analysis could further examine the interplay between blade design parameters and control-system stiffness, δ_3, and other variables.

References

1. Maisel, M. D.; Giulianetti, D. J.; and Dugan, D. C.: The History of the XV-15 Tilt Rotor Research Aircraft: From Concept to Flight. NASA SP-2000-4517.

2. Nixon, M. W.; Piatak, D. J.; Corso, L. M.; Popelka, D. A.: Aeroelastic Tailoring for Stability Augmentation and Performance Enhancements of Tiltrotor Aircraft. Proceedings of NASA Langley Research Center's International Forum on Aeroelasticity and Structural Dynamics, Williamsburg, Virginia, June 22-25, 1999, pp. 121-138.

3. Popelka, D.; Lindsay, D.; Parham, T.; Berry, V.; and Baker, D. J.: Results of an Aeroelastic Tailoring Study for a Composite Tiltrotor Wing. Proceedings 51st Annual Forum of the American Helicopter Society, Fort Worth, Texas, May 1995, vol. II, pp. 1117-1137.

4. Nixon, M. W.: Parametric Studies for Tiltrotor Aeroelastic Stability in High Speed Flight. Journal of the American Helicopter Society, vol. 38, no. 4, October 1993, pp. 71-79.

5. Barkai, S. and Rand, O.: The Influence of Composite Induced Couplings on Tiltrotor Whirl-Flutter Stability. Journal of the American Helicopter Society, vol. 43, no. 2, April 1998, pp. 133-145.

6. van Aken, Johannes M.: Alleviation of Whirl-Flutter on Tilt-Rotor Aircraft Using Active Controls. Proceedings 47th Forum of the American Helicopter Society, Phoenix, Arizona, May 1991, vol. 2, pp. 1321-1344.

7. Matuska, D.; Sacullo, A.; and Studebaker, K.: Reduced Tip Speed Testing of a Variable Diameter Tiltrotor. Proceedings 19th European Rotorcraft Forum, Cernobbio (Como), Italy, September 1993.

8. Srinivas, V.; Chopra, I.; and Nixon, M. W.: Aeroelastic Analysis of Advanced Geometry Tiltrotor Aircraft. Journal of the American Helicopter Society, vol. 43, no. 3, July 1998, pp. 212-221.

9. Detore, J. A. and Gaffey, T. M.: The Stopped-Rotor Variant of the Proprotor VTOL Aircraft. Journal of the American Helicopter Society, vol. 15, no. 3, July 1970, pp. 45-56.

10. Acree, C. W.; Peyran, R. J.; and Johnson, W.: Rotor Design for Whirl Flutter: An Examination of Options for Improving Tiltrotor Aeroelastic Stability Margins. Proceedings 55th Forum of the American Helicopter Society, Montréal, Quebec, Canada, May 1999, vol. 1, pp. 997-1012.

11. Acree, C. W.; Peyran, R. J.; and Johnson, W.: Improving Tiltrotor Whirl-Mode Stability with Rotor Design Variations. Proceedings 26th European Rotorcraft Forum, The Hague, The Netherlands, September 2000.

12. Madden, J. F. III and Peyran, R. J.: Aeroelastic Stability Enhancer for Tilt-Rotor Aircraft. Invention Disclosure, NASA Case No. ARC-14298-1CU, May 1998.

13. Johnson, W.; Lau, B. H.; and Bowles, J. V.: Calculated Performance, Stability, and Maneuverability of High Speed Tilting Proprotor Aircraft. 12th European Rotorcraft Forum, Garmisch-Partenkirchen, Germany, September 1986.

14. Johnson, W.: CAMRAD II Comprehensive Analytical Model of Rotorcraft Aerodynamics and Dynamics—Rotorcraft Applications. Johnson Aeronautics, Palo Alto, California, 1993.

15. Maisel, M.: Tilt Rotor Research Aircraft Familiarization Document. NASA TN X-62,407, January 1975.

16. Johnson, W.: CAMRAD II Comprehensive Analytical Model of Rotorcraft Aerodynamics and Dynamics—Theory Manual. Johnson Aeronautics, Palo Alto, California, 1993.

17. MacNeal-Schwendler Corporation: MSC NASTRAN for Windows—Evaluation Guide and User's Manual. MSC Inc., Los Angeles, California, 1997.

18. Staff of Bell Helicopter Company: Advancement of Proprotor Technology. Task II—Wind-Tunnel Test Results. Bell Helicopter Company Report 300-099-004, NASA CR-114363, September 1971.

19. Johnson, W.: Helicopter Theory. Princeton University Press, 1980.

20. Gaffey, T. M.: The Effect of Positive Pitch-Flap Coupling (Negative δ3) on Rotor Blade Motion Stability and Flapping. Journal of the American Helicopter Society, vol. 14, no. 2, April 1969, pp. 49-67.

21. Chappell, D. P. and Peyran, R. J.: Methodology for Estimating Wing Weights for Conceptual Tilt Rotor and Tilt Wing Aircraft. Society of Allied Weight Engineers 51st Annual Conference, Hartford, Connecticut, May 1992.

22. Staff of Bell Helicopter Company: V/STOL Tilt Rotor Research Aircraft—Volume 3: Structural Loads and Dynamics. Bell Helicopter Co. Report No. 301-199-003, 1974.

23. Wolkovitch, J.; Wainfan, B.; Ben-Harush, Y.; and Johnson, W.: Application of the Joined Wing to Tiltrotor Aircraft. NASA CR-177543, November 1989.

24. Johnson, W.: A Comprehensive Analytical Model of Rotorcraft Aerodynamics and Dynamics. Part I: Analysis Development. NASA TM-81182, June 1980.

25. Rahnke, C.: XV-15 Aerodynamic Model and Blade Tip Acoustic Study. Bell Helicopter Company Report 699-099-507, August 1999.

Appendix A

The CAMRAD II Model of the XV-15

The Fortran namelists below have been simplified for publication. Certain duplicated inputs have been deleted, and most comments deleted or edited. Much of the data have been left in the default format. The number of significant figures is, therefore, neither consistent nor meaningful, being determined by Fortran conventions and the formats of the data sources.

```
 &NLDEF class='CASE',&END
 &NLVAL
     TITLE='NASA/ARMY XV-15 TILTING PROPROTOR AIRCRAFT -- AEROELASTIC STABILITY ANALYSIS',
     CODE='FLUTTER',
     OPUNIT=1,DENSE=.002378,TEMP=59.,
 &END
 !===========================================================================
 &NLDEF class='TRIM',&END
 &NLVAL
     VELIN=1,WINDIN=1,VTIPIN=2,RPM=458.,
     LEVEL=2*1,
     GOV=10.,MTRIM=3,
     MNAME='FORCE X ','FORCE Z ','MOMENT Y',
     VNAME='GOV     ','LNGCYC  ','PITCH   ',
     MHARMR=2*10,MHARMA=2*10,MHARMD=2*10,
     DOFA=6*1,DOFM=10*1,DOFD=8*1,
 &END
 &NLDEF class='TRIM ROTOR',name='ROTOR 1',&END
 &NLVAL
     CNTRLR=22.2,2*0.,
     OPMODE=0,DOFG=1,DOFB=12*1,
     DOFM=12*1,28*0,
 &END
 &NLDEF class='TRIM ROTOR',name='ROTOR 2',&END
 &NLVAL
     CNTRLR=22.2,2*0.,
     OPMODE=0,DOFG=1,DOFB=12*1,
     DOFM=12*1,28*0,
 &END
 !===========================================================================
 &NLDEF class='FLUTTER',&END
 &NLVAL
     DOFA=6*1,DOFM=8*1,2*0,DOFD=8*1,                   ! degrees of freedom
     OPEQN=4*0,2*1,3*0,                    ! symmetric/antisymmetric  equations
 &END
 &NLDEF class='FLUTTER ROTOR',name='ROTOR 1',&END
 &NLVAL
     OPWAKE=3,OPVATR=2,OPVRTA=2,                        ! dynamic inflow
     OPMODE=1,DOFG=1,DOFM=4*1,36*2,DOFL=2,2*0,         ! degrees of freedom
     GDAMPM=40*.06,
 &END
 &NLDEF class='FLUTTER ROTOR',name='ROTOR 2',&END
 &NLVAL
     OPWAKE=3,OPVATR=2,OPVRTA=2,                        ! dynamic inflow
     OPMODE=1,DOFG=1,DOFM=4*1,36*2,DOFL=2,2*0,         ! degrees of freedom
     GDAMPM=40*.06,
 &END
 !===========================================================================
```

Input data for the baseline ("detailed NASTRAN") XV-15 airframe model follow.

```
&NLDEF class='AIRFRAME',type='STRUCTURE',&END
&NLVAL
    TITLE='NASA/ARMY XV-15 TILTING PROPROTOR AIRCRAFT -- AIRFRAME (ATILT = 0, LOCKED)',
    CONFIG=4,ATILT=0.,OPTRAN=1,                           ! tiltrotor
    WEIGHT=13000.,
    IXX=40570.,IYY=13193.,IZZ=50232.,IXZ=98.,
    MASSR=2*12.4311,
    FSCG=24.45,WLCG=6.13,
    FSRTR=25.,BLRTR=16.083,WLRTR=13.0,ASHAFT=2*0.,ACANT=2*1.,
    FSPIV=25.,BLPIV=16.083,WLPIV=8.333,ASPIV=0.,ADPIV=-1.,
    FSWB=24.26,WLWB=8.,
    FSHT=46.67,WLHT=8.58,FSVT=47.5,WLVT=9.64,
    NLOC=17,                                              ! locations
    FSLOC(5)=17.94,WLLOC(5)=4.21,                         !  5=sensor
    FSLOC(6)=23.35,25.18,23.35,  3*46.68,                 !  6-11=wings
    BLLOC(6)=-16.085,0.,16.085, -6.42,0.,6.42,
    WLLOC(6)=8.28,7.72,8.28,      3*8.0,
    FSLOC(12)=21.83,9.33, 25.,17.08, 25.,17.08,           ! 12-17=bodies
    BLLOC(12)=2*0.,        2*-16.083, 2*16.083,
    WLLOC(12)=2*6.78,      2*8.333,   2*8.333,
    HSP=2*2.,OPSPM=0,
    NSEN=1,LOCSEN=5,QUANT=3,OPSCL=1,
    NMODE=10,
    QMASS=241.59,517.75,7.59,63.4,242.69,407.32,113.01,110.83,1386.,353.1,
    QFREQ=3.4,6.6,8.2,19.71,6.3,7.9,7.7,22.853,15.2,21.33,
    ! NASTRAN frequencies = 3.109,6.342,8.155,19.71,6.744,8.723,7.46,22.853,
    QDAMP=.03,.07,.08,.20,.05,.05,.06,.20,.20,.20,
    QSYM=4*1,4*-1,2*1,
    QAEROD=191.9,89.5,11.2,60.7,470.8,2689.6,126.8,137.3,2*0.,
    QAEROC=      62.19000    ,  -42.78000    , 2*0.0000000E+00,
                 1.550000    ,   54.14000    , 2*0.0000000E+00,
                -3.390000    ,   25.75000    , 2*0.0000000E+00,
                -70.32000    ,  -33.48000    , 2*0.0000000E+00,
             2*0.0000000E+00,  -70.10000    ,  -52.62000    ,
             2*0.0000000E+00,   28.50000    ,  -219.2900    ,
             2*0.0000000E+00, -0.9500000    ,   42.19000    ,
             2*0.0000000E+00,  -70.02000    ,   31.01000    ,8*0.,
    ! location1=rotor1(right)
    LSHAPE(1,1,1)=  -1.3700000E-03, -3.3030000E-02, -0.9999900    ,
    LSHAPE(1,1,2)=  -0.9999800    ,  1.031120    ,  1.119680    ,
    LSHAPE(1,1,3)=  -0.1141500    ,  9.9160001E-02, -0.2413100    ,
    LSHAPE(1,1,4)=   0.1759200    ,  0.9999900    , -5.4260001E-02,
    LSHAPE(1,1,5)=  -0.1328900    ,  0.5230800    , -0.8418600    ,
    LSHAPE(1,1,6)=  -0.7699400    ,  0.3644600    , -0.5237900    ,
    LSHAPE(1,1,7)=  -7.6260000E-02, -0.1035000    , -0.9917200    ,
    LSHAPE(1,1,8)=   9.0719998E-02,  1.000000    ,  7.9960003E-02,
    LSHAPE(1,1,9)=  -.0451,             1.,            -.140,
    LSHAPE(1,1,10)=  .1840,             1.,             .649,
    ASHAPE(1,1,1)=  -0.1463200    ,  2.8120000E-02,  2.1700000E-03,
    ASHAPE(1,1,2)=  -6.9780000E-02, -0.3718700    ,  0.2614900    ,
    ASHAPE(1,1,3)=   5.6300000E-03,  7.9999998E-02,  2.6289999E-02,
    ASHAPE(1,1,4)=  -0.1551100    ,  5.3860001E-02,  0.4485000    ,
    ASHAPE(1,1,5)=  -0.1776600    ,  0.1647600    ,  3.8389999E-02,
    ASHAPE(1,1,6)=   0.1011900    ,  0.1913500    ,  0.1780000    ,
    ASHAPE(1,1,7)=   5.6380000E-02,  0.3355700    , -2.2690000E-02,
    ASHAPE(1,1,8)=  -0.3569000    , -7.8160003E-02,  0.6258800    ,
```

```
    ASHAPE(1,1,9)=  -.1160,              .0467,             .332,
    ASHAPE(1,1,10)= -.0356,             -.6000,             .488,
    ! location2=rotor2(left)
    LSHAPE(1,2,1)=  -1.3700000E-03,  3.3030000E-02, -0.9999900     ,
    LSHAPE(1,2,2)=  -0.9999800     , -1.031120     ,  1.119680     ,
    LSHAPE(1,2,3)=  -0.1141500     , -9.9160001E-02, -0.2413100     ,
    LSHAPE(1,2,4)=   0.1759200     , -0.9999900     , -5.4260001E-02,
    LSHAPE(1,2,5)=   0.1328900     ,  0.5230800     ,  0.8418600     ,
    LSHAPE(1,2,6)=   0.7699400     ,  0.3644600     ,  0.5237900     ,
    LSHAPE(1,2,7)=   7.6260000E-02, -0.1035000     ,  0.9917200     ,
    LSHAPE(1,2,8)=  -9.0719998E-02,  1.000000     , -7.9960003E-02,
    LSHAPE(1,2,9)=  -.0451,             -1.,               -.140,
    LSHAPE(1,2,10)=  .1840,             -1.,                .649,
    ASHAPE(1,2,1)=   0.1463200     ,  2.8120000E-02, -2.1700000E-03,
    ASHAPE(1,2,2)=   6.9780000E-02, -0.3718700     , -0.2614900     ,
    ASHAPE(1,2,3)=  -5.6300000E-03,  7.9999998E-02, -2.6289999E-02,
    ASHAPE(1,2,4)=   0.1551100     ,  5.3860001E-02, -0.4485000     ,
    ASHAPE(1,2,5)=  -0.1776600     , -0.1647600     ,  3.8389999E-02,
    ASHAPE(1,2,6)=   0.1011900     , -0.1913500     ,  0.1780000     ,
    ASHAPE(1,2,7)=   5.6380000E-02, -0.3355700     , -2.2690000E-02,
    ASHAPE(1,2,8)=  -0.3569000     ,  7.8160003E-02,  0.6258800     ,
    ASHAPE(1,2,9)=   .1160,              .0467,             -.332,
    ASHAPE(1,2,10)=  .0356,             -.6000,             -.488,
    ! location5=sensor
    LSHAPE(1,5,1)=  -1.3800000E-02,  0.0000000E+00,  0.5048000     ,
    LSHAPE(1,5,2)=   0.7178000     ,  0.0000000E+00,  0.2235000     ,
    LSHAPE(1,5,3)=   3.3500001E-02,  0.0000000E+00,  6.6900000E-02,
    LSHAPE(1,5,4)=  -0.1093000     ,  0.0000000E+00, -0.1384000     ,
    LSHAPE(1,5,5)=   0.0000000E+00, -0.7102000     ,  0.0000000E+00,
    LSHAPE(1,5,6)=   0.0000000E+00, -0.9458000     ,  0.0000000E+00,
    LSHAPE(1,5,7)=   0.0000000E+00,  0.2954000     ,  0.0000000E+00,
    LSHAPE(1,5,8)=   0.0000000E+00,  0.1315000     ,  0.0000000E+00
    LSHAPE(1,5,9)=  -.2870,              0.,               10.480,
    LSHAPE(1,5,10)= -.0973,              0.,                -.129,
&END
&NLDEF class='AIRFRAME',type='AERODYNAMICS',&END
&NLVAL
    LFTAW=880.8,IWBL=3.5,IWBD=3.5,IWBM=-1.95,
    LFTDW=182.8,LFTFW=263.3,
    DRG0W=11.,DRGVW=0.,                    ! vertical drag 241.5
    DRGIW=0.3750938E-3,DRGDW=10.68,DRGFW=4.4,
    AMAXW=17.,
    MOMAW=1253.6,MOMDW=-183.6,MOMFW=-263.5,
    SIDEB=-83.1,ROLLB=166.,ROLLP=-75900.,ROLLR=7900.,ROLLDA=-2901.,
    YAWB=-1291.,YAWP=-1700.,YAWR=-1700.,YAWDA=48.6,
    LFTAH=204.5,LFTEH=117.6,AMAXH=15.,LFTAV=153.,LFTRV=59.1,AMAXV=20.,
    EHTAIL=.49603E-3,LHTAIL=22.,HVTAIL=2.75,
!
    VISRC=2*0,
    NWING=2,LOCWL=6,9,LOCWM=7,10,LOCWR=8,11,
    CIRC=2*0.,FCIRCW=1.,0.,FCIRCH=0.,1.,FCIRCV=0.,0.,AXS=4.30,1.57,
    XCIRC=.19,.25,XTHICK=.27,.375,SPAN=32.17,12.83,CHORD=5.25,3.92,
    NBODY=3,LOCBC=12,14,16,LOCBN=13,15,17,
    LENGTH=25.,2*15.84,THICK=.25,2*.18,SHAPE=3*1,
&END
```

```
&NLDEF class='AIRFRAME',type='CONTROL',&END
&NLVAL
    K0=0.,KC=.194,KS=0.,KP=0.,
    KT=4.,KA=6.288,KE=1.98,KR=5.,
&END
&NLDEF class='AIRFRAME',type='DRIVE TRAIN',&END
&NLVAL
    CONFIG=3,OPGOV=1,
    IGEAR=15.9,EGEAR=35.2,GAINE=10.7,
    KRS=750000.,IRS=2.,
    KIS=4454.42,IIS=2.,
    KES=12000.,
    IENG=.098,DENG=.195,
    KIGOV=.016667,KPGOV=0.,KRGOV=2*1.,KEGOV=0.,
    WGOV=6.2832,ZGOV=.7,
&END
!==============================================================================
&NLDEF class='TABLES',&END
&NLVAL &END
!==============================================================================
&NLDEF action='end of shell',&END
&NLDEF action='end of core',&END

&NLDEF class='ROTOR',type='STRUCTURE',name='ROTOR 1',&END
&NLVAL
    TITLE='NASA/ARMY XV-15 TILTING PROPROTOR AIRCRAFT -- RIGHT ROTOR',
    RADIUS=12.5,NBLADE=3,ROTATE=1,SIGMA=.089,
    VTIPN=600.,
    GIMBAL=1,HINGE=0,
    CONE=2.5,EPITCH=.091,KGMBL=12587.,
    CONTRL=2,PITCH=1,KPITCH=0.,LOCKP=1,
    XSP=.0590,YSP=.017,ZSP=-.16,
    XPH=.0590,YPH=.017,ZPH=.0228,
    EPH=.11,KPL=22400.,LOCKPL=1,LOCKSP=0,
    GDAMPU=.01,GDAMPV=.01,GDAMPW=.01,GDAMPT=.01,
    OPBEAM=2,DRELST=.04,KNODE=2,RNODE=.3,.6,
    NSEN=2,QUANT=2*1,RLOAD=.05,.35,
    NFLAP=0,
    NPROP=51,
    RPROP=0.,.02,.04,.06,.08,.10,.12,.14,.16,.18,.20,
            .22,.24,.26,.28,.30,.32,.34,.36,.38,.40,
            .42,.44,.46,.48,.50,.52,.54,.56,.58,.60,
            .62,.64,.66,.68,.70,.72,.74,.76,.78,.80,
            .82,.84,.86,.88,.90,.92,.94,.96,.98,1.0,
    ZEA=51*0.,ZQC=51*0.,ZC=51*0.,ZI=51*0.,
    XEA=51*0.,XQC=51*0.,XC=51*0.,XI=51*0.,
    XQC=-0.01303,-0.01268,-0.01233,-0.01199,-0.01164,-0.01129,
        -0.01095,-0.01060,-0.01026,-0.00991,-0.00956,
        -0.00922,-0.00887,-0.00852,-0.00815,-0.00778,
        -0.00742,-0.00705,-0.00671,-0.00638,-0.00605,
        -0.00572,-0.00539,-0.00506,-0.00471,-0.00436,
        -0.00402,-0.00367,-0.00332,-0.00297,-0.00262,
        -0.00227,-0.00193,-0.00160,-0.00127,-0.00092,
        -0.00055,-0.00019,0.00017,0.00052,0.00088,
         0.00122,0.00157,0.00191,0.00225,0.00260,
         0.00300,0.00335,0.00368,0.00402,0.00435,
    XI      = 2*3.3000001E-04,  6.5000000E-04,  1.0800000E-03,  1.5100000E-03,
                1.9300000E-03,  2.3600000E-03,  2.8500000E-03,  3.3499999E-03,
```

```
                 3.9300001E-03,   4.6999999E-03,   5.4700002E-03,   6.4900001E-03,
                 7.5800000E-03,   9.0300003E-03,   1.1530000E-02,   1.4040000E-02,
                 1.1210000E-02,   6.5899999E-03,3*3.1300001E-03,   2.5000001E-04,
                -3.5900001E-03,  -6.3900002E-03,  -6.0700001E-03,  -5.7500000E-03,
                -5.4500001E-03,  -5.1500001E-03,  -4.8500001E-03,  -4.5300000E-03,
                -4.2099999E-03,  -3.8900001E-03,  -3.5699999E-03,  -3.2500001E-03,
                -2.9000000E-03,  -2.5500001E-03,  -2.1899999E-03,  -1.8100000E-03,
                -1.4400000E-03,  -1.0700000E-03,  -6.9000002E-04,  -2.8000001E-04,
                 1.5000001E-04,   5.7999999E-04,   1.0300000E-03,   1.4900001E-03,
                 2.0200000E-03,   2.5800001E-03,2*3.0000000E-03,
XC       = 2*3.3000001E-04,   6.5000000E-04,   1.0800000E-03,   1.5100000E-03,
                 1.9300000E-03,   2.3600000E-03,   2.8500000E-03,   3.3499999E-03,
                 3.9300001E-03,   4.6999999E-03,   5.4700002E-03,   6.4900001E-03,
                 7.5800000E-03,   9.0300003E-03,   1.1530000E-02,   1.4040000E-02,
                 1.1210000E-02,   6.5899999E-03,3*3.1300001E-03,   2.5000001E-04,
                -3.5900001E-03,  -6.3900002E-03,  -6.0700001E-03,  -5.7500000E-03,
                -5.4500001E-03,  -5.1500001E-03,  -4.8500001E-03,  -4.5300000E-03,
                -4.2099999E-03,  -3.8900001E-03,  -3.5699999E-03,  -3.2500001E-03,
                -2.9000000E-03,  -2.5500001E-03,  -2.1899999E-03,  -1.8100000E-03,
                -1.4400000E-03,  -1.0700000E-03,  -6.9000002E-04,  -2.8000001E-04,
                 1.5000001E-04,   5.7999999E-04,   1.0300000E-03,   1.4900001E-03,
                 2.0200000E-03,   2.5800001E-03,2*3.0000000E-03,
TWISTA   =   34.43,33.49,32.45,31.55,30.79,30.03,29.03,28.03,26.88,
             25.58,24.28,23.03,21.78,20.43,18.98,17.53,16.48,15.43,
             14.20,12.79,11.38,10.64,9.9,9.03,8.03,7.03,6.43,5.83,
             5.19,4.51,3.83,3.31,2.79,2.3,1.84,1.38,0.83,0.27,
             -0.27,-0.82,-1.37,-1.86,-2.35,-2.82,-3.27,-3.72,-4.14,
             -4.56,-4.98,-5.4,-5.82,
THETAC   =   34.43,33.49,32.45,31.55,30.79,30.03,29.03,28.03,26.88,
             25.58,24.28,23.03,21.78,20.43,18.98,17.53,16.48,15.43,
             14.20,12.79,11.38,10.64,9.9,9.03,8.03,7.03,6.43,5.83,
             5.19,4.51,3.83,3.31,2.79,2.3,1.84,1.38,0.83,0.27,
             -0.27,-0.82,-1.37,-1.86,-2.35,-2.82,-3.27,-3.72,-4.14,
             -4.56,-4.98,-5.4,-5.82,
THETAI   =   34.43,33.49,32.45,31.55,30.79,30.03,29.03,28.03,26.88,
             25.58,24.28,23.03,21.78,20.43,18.98,17.53,16.48,15.43,
             14.20,12.79,11.38,10.64,9.9,9.03,8.03,7.03,6.43,5.83,
             5.19,4.51,3.83,3.31,2.79,2.3,1.84,1.38,0.83,0.27,
             -0.27,-0.82,-1.37,-1.86,-2.35,-2.82,-3.27,-3.72,-4.14,
             -4.56,-4.98,-5.4,-5.82,
KP =   .0069,.0183,.0158,.0135,.0120,.0117,.0114,.0123,
       .0148,.0202,.0217,.0233,.0247,.0260,.0275,.0295,
       .0315,.0320,.0320,.0317,.0309,.0301,.0287,.0273,
       .0263,.0262,.0261,.0260,.0258,.0257,.0255,.0254,
       .0253,.0251,.0250,.0248,.0247,.0247,.0246,.0246,
       .0246,.0245,.0245,.0245,.0245,.0246,.0247,.0233,
       .0218,2*.0192,
KT =   .0069,.0183,.0158,.0135,.0120,.0117,.0114,.0123,
       .0148,.0202,.0217,.0233,.0247,.0260,.0275,.0295,
       .0315,.0320,.0320,.0317,.0309,.0301,.0287,.0273,
       .0263,.0262,.0261,.0260,.0258,.0257,.0255,.0254,
       .0253,.0251,.0250,.0248,.0247,.0247,.0246,.0246,
       .0246,.0245,.0245,.0245,.0245,.0246,.0247,.0233,
       .0218,2*.0192,
EA=51*30000000.,
EIFLAP   = 4*1111000.    ,   1215000.    ,   1632000.    ,   2049000.     ,
             1911000.    ,   1589000.    ,   1287000.    ,   1045000.     ,
             803000.0    ,   674000.0    ,   582000.0    ,   499000.0     ,
```

```
                445000.0      ,      392000.0     ,      355000.0     ,      323000.0     ,
                294000.0      ,      278000.0     ,      261000.0     ,      246000.0     ,
                232000.0      ,      217000.0     ,      202000.0     ,      188000.0     ,
                175000.0      ,      163000.0     ,      151000.0     ,      140000.0     ,
                129000.0      ,      120000.0     ,      110000.0     ,      101000.0     ,
                93400.00      ,      85300.00     ,      78100.00     ,      71200.00     ,
                64400.00      ,      58300.00     ,      52200.00     ,      47200.00     ,
                42400.00      ,      37800.00     ,      33700.00     ,      29500.00     ,
                26100.00      ,      22800.00     , 2*20400.00     ,
 EILAG   = 4*1111000.       ,      1259000.     ,      1851000.     ,      2440000.     ,
                3070000.      ,      3720000.     ,      4250000.     ,      4470000.     ,
                4680000.      ,      5060000.     ,      5480000.     ,      5660000.     ,
                5100000.      ,      4530000.     ,      3980000.     ,      3440000.     ,
                3060000.      ,      3160000.     ,      3250000.     ,      3490000.     ,
                3770000.      ,      3960000.     ,      3870000.     ,      3790000.     ,
                3690000.      ,      3600000.     ,      3500000.     ,      3410000.     ,
                3320000.      ,      3230000.     ,      3150000.     ,      3060000.     ,
                2990000.      ,      2910000.     ,      2850000.     ,      2780000.     ,
                2710000.      ,      2650000.     ,      2590000.     ,      2530000.     ,
                2470000.      ,      2420000.     ,      2370000.     ,      2320000.     ,
                2280000.      ,      2240000.     , 2*2210000.     ,
 GJ      = 2*410000.0      ,      357000.0     ,      287000.0     ,      256000.0     ,
                344000.0      ,      432000.0     ,      403000.0     ,      335000.0     ,
                271000.0      ,      220000.0     ,      170000.0     ,      142200.0     ,
                122400.0      ,      104900.0     ,      93700.00     ,      82600.00     ,
                74800.00      ,      68000.00     ,      62000.00     ,      58500.00     ,
                55000.00      ,      51900.00     ,      48800.00     ,      45700.00     ,
                42600.00      ,      39500.00     ,      36800.00     ,      34200.00     ,
                31700.00      ,      29500.00     ,      27200.00     ,      24800.00     ,
                22300.00      ,      20200.00     ,      19000.00     ,      17900.00     ,
                16500.00      ,      15000.00     ,      13570.00     ,      12290.00     ,
                11010.00      ,      9940.000     ,      8940.000     ,      7980.000     ,
                7100.000      ,      6230.000     ,      5500.000     ,      4820.000     ,
                2*4310.000      ,
 MASS    =    4.513000      ,     0.6380000    ,     0.8070000    ,      1.032000     ,
                1.192000      ,     1.156000     ,     1.120000     ,     0.8530000    ,
               0.5080000      ,    0.2460000    ,    0.2310000    ,    0.2160000    ,
               0.2080000      ,    0.2020000    ,    0.1950000    ,    0.1840000    ,
               0.1740000      ,    0.1640000    ,    0.1530000    ,    0.1460000    ,
               0.1520000      ,    0.1570000    ,    0.1710000    ,    0.1890000    ,
               0.2010000      ,    0.1970000    ,    0.1930000    ,    0.1890000    ,
               0.1860000      ,    0.1820000    ,    0.1790000    ,    0.1750000    ,
               0.1710000      ,    0.1680000    ,    0.1640000    ,    0.1610000    ,
               0.1570000      ,    0.1540000    ,    0.1500000    ,    0.1470000    ,
               0.1430000      ,    0.1400000    ,    0.1360000    ,    0.1320000    ,
               0.1290000      ,    0.1250000    ,    0.1220000    ,    0.1330000    ,
               0.1490000      ,2*0.1610000    ,
 ITHETA  = 2*3.3399999E-02,  3.1700000E-02,  2.9300001E-02,  2.7000001E-02,
               2.4800001E-02,  2.2600001E-02,  2.0099999E-02,  1.7400000E-02,
               1.5699999E-02,  1.7000001E-02,  1.8400000E-02,  1.9800000E-02,
               2.1400001E-02,  2.3000000E-02,  2.5000000E-02,  2.7000001E-02,
               2.6200000E-02,  2.4400000E-02,  2.3000000E-02,  2.2600001E-02,
               2.2200000E-02,2*2.2000000E-02,  2.1800000E-02,  2.1100000E-02,
               2.0500001E-02,  1.9900000E-02,  1.9300001E-02,  1.8700000E-02,
               1.8200001E-02,  1.7600000E-02,  1.7100001E-02,  1.6500000E-02,
               1.6000001E-02,  1.5500000E-02,  1.5000000E-02,  1.4600000E-02,
               1.4200000E-02,  1.3900000E-02,  1.3500000E-02,  1.3100000E-02,
               1.2800000E-02,  1.2400000E-02,  1.2100000E-02,  1.1800000E-02,
```

```
                1.1600000E-02,  1.1300000E-02,  1.1100000E-02,2*1.1000000E-02,
    IPOLAR  = 2*3.3399999E-02,  3.1700000E-02,  2.9300001E-02,  2.7000001E-02,
                2.4800001E-02,  2.2600001E-02,  2.0099999E-02,  1.7400000E-02,
                1.5699999E-02,  1.7000001E-02,  1.8400000E-02,  1.9800000E-02,
                2.1400001E-02,  2.3000000E-02,  2.5000000E-02,  2.7000001E-02,
                2.6200000E-02,  2.4400000E-02,  2.3000000E-02,  2.2600001E-02,
                2.2200000E-02,2*2.2000000E-02,  2.1800000E-02,  2.1100000E-02,
                2.0500001E-02,  1.9900000E-02,  1.9300001E-02,  1.8700000E-02,
                1.8200001E-02,  1.7600000E-02,  1.7100001E-02,  1.6500000E-02,
                1.6000001E-02,  1.5500000E-02,  1.5000000E-02,  1.4600000E-02,
                1.4200000E-02,  1.3900000E-02,  1.3500000E-02,  1.3100000E-02,
                1.2800000E-02,  1.2400000E-02,  1.2100000E-02,  1.1800000E-02,
                1.1600000E-02,  1.1300000E-02,  1.1100000E-02,2*1.1000000E-02,
&END
!===============================================================================
&NLDEF class='ROTOR',type='AERODYNAMICS',name='ROTOR 1',&END
&NLVAL
    NPANEL=15,
    REDGE=.1,.2,.3,.4,.5,.6,.66,.72,.77,.81,.85,.88,.91,.94,.97,1.,
    NPROP=5,RPROP=0.,.1,.2,.3,1.,
    CHORD=2*1.32125,1.17375,2*1.16625,
    NSEN=5,OPREF=5*4,                              ! aerodynamic sensors
    QUANT= 5,25,35,82,82,                          !   lambda
    IDENT= 1, 0, 0, 0, 0,                          !   alpha, theta
    AXIS=  3, 0, 0, 1, 3,                          !   Fx, Fz
    OPSCL= 2, 1, 1, 2, 2,                          !
    NAPLOT=1, 4, 1, 0, 0,                          !
&END
!===============================================================================
&NLDEF class='ROTOR',type='INFLOW',name='ROTOR 1',&END
&NLVAL
    KHLMDA=1.085,KFLMDA=2.,FMLMDA=0.,
    KINTFR(2)=-.085,KINTHW=1.5,KINTFH=1.8,
&END
&NLDEF class='ROTOR',type='WAKE',name='ROTOR 1',&END
&NLVAL
    OPSCEN=2,TWIST=-22.,                           ! hover wake
&END
&NLDEF class='ROTOR',type='WAKE',name='ROTOR 1',&END
&NLVAL OPSCEN=0,RNW=.25,OPAX=0,WKMODL=8*2,&END
!===============================================================================
&NLDEF action='end of shell',&END
&NLDEF action='end of core',&END


&NLDEF class='ROTOR',type='STRUCTURE',name='ROTOR 2',&END
&NLVAL
    TITLE='NASA/ARMY XV-15 TILTING PROPROTOR AIRCRAFT -- LEFT ROTOR',
    RADIUS=12.5,NBLADE=3,ROTATE=-1,SIGMA=.089,
&END
&NLDEF class='ROTOR',type='INFLOW',name='ROTOR 2',&END
&NLVAL
    KHLMDA=1.085,KFLMDA=2.,FMLMDA=0.,
    KINTFR(1)=-.085,KINTHW=1.5,KINTFH=1.8,
&END
```

All other ROTOR 2 parameters are identical to those of ROTOR 1.

Input data from the "thick-wing" NASTRAN stick model follow. All other parameters are identical to those of the baseline model.

```
&NLDEF class='CASE',&END
&NLVAL
    TITLE='XV-15 WITH STICK MODEL MODES -- AEROELASTIC STABILITY ANALYSIS',
&END
&NLDEF class='AIRFRAME',type='STRUCTURE',&END
&NLVAL
    TITLE='XV-15 WITH STICK MODEL MODES (ATILT = 0, LOCKED)',
!  Mode shapes and frequencies from MSC NASTRAN for Windows "Stick" Model
    NMODE=6,
    MENAME=  'Symmetric wing beam bending',
             'Symmetric wing chord bending',
             'Symmetric wing torsion',
             'Antisymmetric wing beam bending',
             'Antisymmetric wing chord bending',
             'Antisymmetric wing torsion',
    MELABL=  'SWB', 'SWC', 'SWT', 'AWB', 'AWC', 'AWT',
!****Frequencies from NASTRAN for Windows Stick Model
   QFREQ=  3.293,  6.320,  8.340,  6.267,  7.075,  8.703,
!****Masses from NASTRAN for Windows Stick Model
   QMASS=201.611, 319.965, 50.109, 231.637, 242.992, 57.764,
!***Mode shapes right hub from NASTRAN for Windows
 LSHAPE(1,1,1)=-0.274534E-01, 0.641842E-01, 0.100000E+01,
 LSHAPE(1,1,2)= 0.100000E+01,-0.928248E+00,-0.275460E+00,
 LSHAPE(1,1,3)=-0.184042E+00, 0.123503E+00,-0.552480E+00,
 LSHAPE(1,1,4)= 0.270239E+00,-0.304366E+00, 0.943833E+00,
 LSHAPE(1,1,5)= 0.707744E+00,-0.398595E+00,-0.576665E+00,
 LSHAPE(1,1,6)=-0.249960E+00, 0.802357E-01,-0.451574E+00,
 ASHAPE(1,1,1)= 0.138543E+00,-0.250751E-01, 0.251207E-02,
 ASHAPE(1,1,2)= 0.321882E-01, 0.112465E+00,-0.190338E+00,
 ASHAPE(1,1,3)= 0.405354E-01, 0.202698E+00, 0.219114E-01,
 ASHAPE(1,1,4)= 0.100003E+00,-0.156089E+00,-0.304170E-01,
 ASHAPE(1,1,5)= 0.212266E-01, 0.195098E+00,-0.124386E+00,
 ASHAPE(1,1,6)= 0.651168E-01, 0.189523E+00, 0.308434E-01,
!***Mode shapes left hub from NASTRAN for Windows
 LSHAPE(1,2,1)=-0.274534E-01,-0.641842E-01, 0.100000E+01,
 LSHAPE(1,2,2)= 0.100000E+01, 0.928248E+00,-0.275460E+00,
 LSHAPE(1,2,3)=-0.184042E+00,-0.123503E+00,-0.552480E+00,
 LSHAPE(1,2,4)=-0.270239E+00,-0.304366E+00,-0.943833E+00,
 LSHAPE(1,2,5)=-0.707744E+00,-0.398595E+00, 0.576665E+00,
 LSHAPE(1,2,6)= 0.249960E+00, 0.802357E-01, 0.451574E+00,
 ASHAPE(1,2,1)=-0.138543E+00,-0.250751E-01,-0.251207E-02,
 ASHAPE(1,2,2)=-0.321882E-01, 0.112465E+00, 0.190338E+00,
 ASHAPE(1,2,3)=-0.405354E-01, 0.202698E+00,-0.219114E-01,
 ASHAPE(1,2,4)= 0.100003E+00, 0.156089E+00,-0.304170E-01,
 ASHAPE(1,2,5)= 0.212266E-01,-0.195098E+00,-0.124386E+00,
 ASHAPE(1,2,6)= 0.651168E-01,-0.189523E+00, 0.308434E-01,
! No aerodynamic damping:
  QAEROD=6*0.0,QAEROC=40*0.0,
    QSYM=3*1,3*-1,
  QDAMP=.03,.07,.08,.05,.05,.06,
&END
```

Input data from the "thin-wing" NASTRAN stick model follow. All other parameters are identical to those of the baseline model.

```
 &NLDEF class='CASE',&END
 &NLVAL
      TITLE='XV-15 WITH THIN WING -- AEROELASTIC STABILITY ANALYSIS [12/98]',
      CODE='FLUTTER',
      OPUNIT=1,DENSE=.002378,TEMP=59.,
 &END

 &NLDEF class='AIRFRAME',type='STRUCTURE',&END
 &NLVAL
      TITLE='XV-15 WITH R. PEYRAN''S THIN WING (ATILT = 0, LOCKED) [12/98]',
      NMODE=6,
      QSYM=3*1,3*-1,
!****Frequencies from NASTRAN for Windows Stick Model
      QFREQ= 2.424, 5.104, 5.974, 4.570, 6.522, 5.484,
!****Masses from NASTRAN for Windows Stick Model
      QMASS=194.819, 154.612, 66.537, 199.105,117.104, 86.614,
!****Zero out aerodynamic damping (conservative, plus varies with mode shape)
      QAEROD= 0., 0., 0., 0., 0., 0.,
!****Zero out QAEROC
      QAEROC= 40*0.,
!****Damping for six wing modes
      QDAMP= .03, .07, .08, .05, .05, .06,
!***Mode shapes at right hub from NASTRAN for Windows
      LSHAPE(1,1,1)=-0.247409E-01, 0.619576E-01, 0.100000E+01,
      LSHAPE(1,1,2)=0.540728E+00,-0.533949E+00,-0.507410E+00,
      LSHAPE(1,1,3)=-0.359734E+00,0.281981E+00,-0.544684E+00,
      LSHAPE(1,1,4)= 0.152875E+00,-0.223944E+00,0.100000E+01,
      LSHAPE(1,1,5)= 0.550376E+00,-0.231849E+00, 0.417617E+00,
      LSHAPE(1,1,6)=-0.267452E+00, 0.200962E+00, 0.431073E+00,
      ASHAPE(1,1,1)=0.136220E+00,-0.288973E-01, 0.223698E-02,
      ASHAPE(1,1,2)= 0.480945E-01,0.196812E+00,-0.111702E+00,
      ASHAPE(1,1,3)= 0.406928E-01, 0.201679E+00,0.539970E-01,
      ASHAPE(1,1,4)= 0.795902E-01,-0.195246E+00,-0.948505E-02,
      ASHAPE(1,1,5)=-0.753927E-01,-0.185089E+00,-0.791143E-01,
      ASHAPE(1,1,6)=-0.594299E-01,-0.186845E+00, 0.522021E-01,
!***Mode shapes left hub from NASTRAN for Windows
      LSHAPE(1,2,1)=-0.247409E-01,-0.619576E-01,0.100000E+01,
      LSHAPE(1,2,2)= 0.540728E+00, 0.533949E+00,-0.507410E+00,
      LSHAPE(1,2,3)=-0.359734E+00,-0.281981E+00,-0.544684E+00,
      LSHAPE(1,2,4)=-0.152875E+00,-0.223944E+00,-0.100000E+01,
      LSHAPE(1,2,5)=-0.550376E+00,-0.231849E+00,-0.417617E+00,
      LSHAPE(1,2,6)=0.267452E+00, 0.200962E+00,-0.431073E+00,
      ASHAPE(1,2,1)=-0.136220E+00,-0.288973E-01,-0.223698E-02,
      ASHAPE(1,2,2)=-0.480945E-01, 0.196812E+00, 0.111702E+00,
      ASHAPE(1,2,3)=-0.406928E-01, 0.201679E+00,-0.539970E-01,
      ASHAPE(1,2,4)=0.795902E-01, 0.195246E+00,-0.948505E-02,
      ASHAPE(1,2,5)=-0.753927E-01,0.185089E+00,-0.791143E-01,
      ASHAPE(1,2,6)=-0.594299E-01, 0.186845E+00,0.522021E-01,
 &END
 &NLDEF class='AIRFRAME',type='AERODYNAMICS',&END
 &NLVAL
! 75% flat-plate drag for thin wing:
      DRG0W=8.25, DRGVW=0.,                  !  vertical drag 241.5
 &END
```

Inputs for airfoil tables (interpolated) follow. The airfoil boundaries specified as follows are believed to more accurately represent the XV-15 than the boundaries given at the end of each table.

```
&NLTABL OPFORM=2,RNTRP=0,
      TITLE='XV-15 ROTOR AIRFOILS (64X28/18/12/08) (C81 TABLES; INTERPOLATED SPANWISE)',
      NRB=4,R=.2,.55,.8,.95,
 &END
```

C81 table for the first blade segment (0.2–0.55 *R*):

```
64-X25  2-D  AERODYNAMICS      323 323 323
         0.0    0.45   0.75
-180.  -.35   -.35   -.35
-90.    0.0    0.0    0.0
-45.   -1.0   -1.0   -1.0
-10.   -.55   -.50   -.275
-8.0   -.49   -.445  -.215
-6.0   -.325  -.29   -.15
-4.0   -.15   -.13   -.055
-2.0    .038   .04    .03
0.0     .26    .26    .12
2.0     .48    .485   .205
4.0     .70    .70    .290
6.0     .935   .935   .405
8.0    1.01   1.01    .435
10.0   1.105  1.105   .46
12.0   1.125  1.12    .48
14.    1.12   1.125   .50
16.    1.125  1.125   .52
20.    1.170  1.170   .70
24.    1.26   1.26   1.0
30.    1.42   1.42   1.3
45.    1.45   1.45   1.45
90.     0.0    0.0    0.0
180.    .35    .35    .35
         0.0    0.55   0.75
-180.   .019   .019   .11
-90.   2.1    2.1    2.1
-45.   1.2    1.2    1.3
-10.    .023   .06    .278
-8.0    .017   .043   .206
-6.0    .014   .03    .168
-4.0    .014   .014   .139
-2.0    .014   .014   .12
0.0     .014   .014   .12
2.0     .014   .014   .12
4.0     .014   .014   .135
6.0     .026   .026   .15
8.0     .028   .028   .20
10.     .034   .034   .28
12.     .042   .042   .37
14.     .06    .06    .45
16.     .10    .10    .56
20.     .174   .174   .75
24.     .25    .25    .98
30.     .50    .50    .65
45.    1.2    1.2    1.3
```

28

90.	2.1	2.1	2.1
180.	.019	.019	.110
	0.0	.45	0.75
−180.	−.19	−.19	−.17
−90.	−.5	−.5	−.5
−45.	.5	.5	.5
−10.	−.075	−.075	−.075
−8.	−.075	−.075	−.075
−6.	−.075	−.075	−.075
−4.	−.075	−.075	−.075
−2.	−.075	−.075	−.075
0.0	−.075	−.075	−.075
2.0	−.075	−.075	−.075
4.0	−.075	−.075	−.078
6.0	−.075	−.075	−.105
8.0	−.075	−.075	−.130
10.	−.075	−.075	−.150
12.	−.075	−.075	−.180
14.	−.075	−.11	−.21
16.	−.15	−.18	−.24
20.	−.20	−.21	−.28
24.	−.22	−.24	−.30
30.	−.24	−.28	−.32
45.	−.5	−.5	−.5
90.	.50	.50	.50
180.	.04	.04	.04

CLCD3015 for XV–15, RLM 4/30/75, r = 0.−.45

C81 table for the second blade segment (0.55–0.8 *R*):

64−X18 2−D AERODYNAMICS				923 923 923				
	0.0	0.3	0.4	0.42	0.50	0.52	0.60	0.66	0.71
−180.	−.1	−.1	−.1	−.1	−.1	−.1	−.1	−.1	−.1
−90.	0.0	0.0	0.0	0.0	0.0	0.0	0.0	0.0	0.0
−45.	−1.0	−1.0	−1.0	−1.0	−1.0	−1.0	−1.0	−1.0	−1.0
−10.	−1.051	−1.051	−1.042	−1.042	−.902	−.902	−.90	−.85	−.70
−8.0	−.847	−.847	−.869	−.869	−.851	−.851	−.855	−.780	−.60
−6.0	−.679	−.679	−.635	−.635	−.656	−.656	−.630	−.575	−.469
−4.0	−.408	−.408	−.410	−.410	−.419	−.419	−.403	−.359	−.281
−2.0	−.175	−.175	−.178	−.178	−.183	−.183	−.172	−.140	−.147
0.0	.033	.033	.035	.035	.033	.033	.025	.012	−.008
2.0	.252	.252	.261	.261	.268	.268	.243	.203	.099
4.0	.487	.487	.502	.502	.514	.514	.473	.413	.319
6.0	.702	.703	.720	.720	.728	.728	.688	.623	.510
8.0	.918	.918	.933	.933	.940	.940	.897	.808	.673
10.0	1.076	1.076	1.086	1.086	.972	.972	1.025	.915	.782
12.0	1.199	1.199	1.124	1.124	1.045	1.045	1.086	.972	.850
14.0	1.173	1.173	1.076	1.076	1.093	1.093	1.027	.989	.850
16.0	1.150	1.150	.987	.987	1.009	1.009	.98	1.00	.850
20.	1.140	1.140	.920	.920	.980	.980	.950	1.03	.920
24.	1.130	1.130	1.01	1.01	1.02	1.02	1.01	1.05	1.01
30.	1.140	1.140	1.12	1.12	1.12	1.12	1.12	1.12	1.12
45.	1.2	1.2	1.2	1.2	1.2	1.2	1.2	1.2	1.2
90.0	0.0	0.0	0.0	0.0	0.0	0.0	0.0	0.0	0.0

```
180.     .10     .10     .10     .10     .10     .10     .10     .10     .10
         0.0     .3      .4      .42     .50     .52     .60     .66     .71
-180.    .016    .016    .015    .015    .014    .014    .013    .010    .012
-90.     2.1     2.1     2.1     2.1     2.1     2.1     2.1     2.1     2.1
-45.     1.1     1.1     1.1     1.1     1.1     1.1     1.1     1.1     1.1
-10.     .016    .016    .016    .016    .058    .058    .09     .12     .16
-8.0     .012    .012    .012    .012    .016    .016    .022    .025    .060
-6.0     .011    .011    .010    .010    .011    .011    .011    .009    .035
-4.0     .010    .010    .009    .009    .009    .009    .008    .008    .017
-2.0     .007    .007    .007    .007    .007    .007    .007    .007    .016
0.0      .007    .007    .007    .007    .007    .007    .007    .007    .017
2.0      .007    .007    .007    .007    .007    .007    .007    .007    .019
4.0      .006    .006    .008    .008    .007    .007    .007    .008    .028
6.0      .01     .01     .01     .01     .01     .01     .007    .013    .051
8.0      .013    .013    .014    .014    .015    .015    .014    .037    .072
10.      .019    .019    .034    .022    .070    .070    .032    .082    .137
12.      .077    .077    .092    .070    .084    .090    .067    .10     .14
14.      .105    .105    .113    .100    .11     .12     .12     .12     .16
16.      .134    .134    .140    .140    .150    .150    .170    .22     .26
20.      .210    .210    .22     .22     .23     .23     .28     .33     .37
24.      .310    .310    .32     .32     .33     .33     .38     .43     .47
30.      .476    .476    .485    .485    .498    .498    .55     .60     .65
45.      1.1     1.1     1.1     1.1     1.1     1.1     1.1     1.1     1.1
90.      2.1     2.1     2.1     2.1     2.1     2.1     2.1     2.1     2.1
180.     .016    .016    .015    .015    .014    .014    .013    .010    .012
         0.0     0.3     0.4     0.42    0.5     0.52    0.6     0.66    0.71
-180.    -.14    -.14    -.14    -.14    -.135   -.135   -.122   -.122   -.11
-90.     -.5     -.5     -.5     -.5     -.5     -.5     -.5     -.5     -.5
-45.     .5      .5      .5      .5      .5      .5      .5      .5      .5
-10.     -.011   -.011   -.014   -.014   -.017   -.017   .019    .020    .04
-8.      -.01    -.01    -.011   -.011   -.014   -.014   -.019   -.02    0.0
-6.      -.008   -.008   -.009   -.009   -.009   -.009   -.007   -.009   -.002
-4.      -.008   -.008   -.008   -.008   -.008   -.008   -.007   -.007   -.009
-2.      -.008   -.008   -.008   -.008   -.008   -.008   -.008   -.009   -.032
0.0      -.008   -.008   -.008   -.008   -.008   -.008   -.008   -.008   -.008
2.0      -.009   -.009   -.009   -.009   -.010   -.010   -.013   -.012   -.009
4.0      -.01    -.01    -.01    -.01    -.012   -.012   -.014   -.014   -.018
6.0      -.01    -.01    -.011   -.011   -.013   -.013   -.014   -.013   -.026
8.0      -.008   -.008   -.008   -.008   -.008   -.008   -.008   -.019   -.034
10.      -.006   -.006   -.008   -.008   -.011   -.011   -.005   -.034   -.063
12.      -.015   -.015   -.015   -.015   -.15    -.15    -.013   -.054   -.127
14.      -.019   -.019   -.018   -.018   0.0     0.0     -.056   -.081   -.158
16.      -.025   -.025   -.028   -.028   -.053   -.053   -.18    -.18    -.188
20.      -.18    -.18    -.18    -.18    -.18    -.18    -.20    -.20    -.20
24.      -.20    -.20    -.20    -.20    -.20    -.20    -.24    -.24    -.24
30.      -.20    -.23    -.25    -.25    -.27    -.27    -.28    -.28    -.28
45.      -.5     -.5     -.5     -.5     -.5     -.5     -.5     -.5     -.5
90.      .5      .5      .5      .5      .5      .5      .5      .5      .5
180.     .09     .09     .087    .087    .085    .085    .08     .072    .066
```

CLCD3016 for XV-15, RLM 4/30/75, r = .45-.7

C81 table for the third blade segment (0.8–0.95 *R*):

```
64-X12 2-D  AERODYNAMICS     122312231223
       0.0    0.3    0.4    0.42   0.5    0.52   0.6    0.66   0.71
       0.76   0.81   0.85
-180.  -.1    -.1    -.1    -.1    -.1    -.1    -.1    -.1    -.1
       -.1    -.1    -.1
-90.   0.0    0.0    0.0    0.0    0.0    0.0    0.0    0.0    0.0
       0.0    0.0    0.0
-45.   -1.0   -1.0   -1.0   -1.0   -1.0   -1.0   -1.0   -1.0   -1.0
       -1.0   -1.0   -1.0
-10.   -.767  -.767  -.741  -.741  -.706  -.706  -.495  -.58   -.87
       -.80   -.73   -.49
-8.0   -.708  -.708  -.708  -.708  -.70   -.70   -.72   -.883  -.818
       -.772  -.710  -.55
-6.0   -.559  -.559  -.589  -.589  -.587  -.587  -.626  -.656  -.659
       -.595  -.585  -.440
-4.0   -.343  -.343  -.357  -.357  -.380  -.380  -.405  -.414  -.425
       -.396  -.375  -.310
-2.0   -.123  -.123  -.125  -.125  -.132  -.132  -.146  -.155  -.160
       -.144  -.160  -.155
0.0    .078   .078   .085   .085   .089   .089   .093   .099   .099
       .072   .059   .050
2.0    .309   .309   .318   .318   .338   .338   .363   .373   .362
       .331   .270   .228
4.0    .523   .523   .551   .551   .583   .583   .627   .623   .604
       .537   .485   .410
6.0    .735   .735   .781   .781   .825   .825   .883   .874   .797
       .709   .660   .600
8.0    .956   .956   1.012  1.012  1.020  1.020  1.054  1.017  .948
       .82    .810   .780
10.0   1.1    1.1    1.125  1.125  1.095  1.13   1.145  1.085  1.057
       .91    .93    .960
12.0   1.154  1.154  1.086  1.086  1.006  1.16   1.044  1.046  1.142
       .97    .97    1.00
14.0   .945   .945   .977   .977   .959   1.13   .958   1.066  1.08
       1.01   1.01   1.01
16.0   .800   .800   .803   .803   .925   1.02   .930   1.08   1.04
       1.04   1.04   1.04
20.0   .910   .910   .920   .920   .920   .920   .930   1.12   1.02
       1.08   1.08   1.08
24.0   1.01   1.01   1.01   1.01   1.01   1.01   1.01   1.15   1.05
       1.10   1.10   1.10
30.0   1.12   1.12   1.12   1.12   1.12   1.12   1.12   1.18   1.12
       1.12   1.12   1.12
45.0   1.2    1.2    1.2    1.2    1.2    1.2    1.2    1.2    1.2
       1.2    1.2    1.2
90.0   0.0    0.0    0.0    0.0    0.0    0.0    0.0    0.0    0.0
       0.0    0.0    0.0
180.   .10    .10    .10    .10    .10    .10    .10    .10    .10
       .10    .10    .10
       0.0    0.3    0.4    0.42   0.5    0.52   0.6    0.66   0.71
       0.76   0.81   0.85
-180.  .017   .016   .017   .015   .014   .014   .013   .012   .011
       .05    .11    .11
-90.   2.1    2.1    2.1    2.1    2.1    2.1    2.1    2.1    2.1
       2.1    2.1    2.1
```

−45.	1.1	1.1	1.1	1.1	1.1	1.1	1.1	1.1	1.1		
	1.2	1.3	1.4								
−10.	.149	.149	.132	.132	.135	.135	.153	.184	.231		
	.282	.33	.37								
−8.0	.059	.059	.068	.068	.080	.080	.058	.066	.098		
	.143	.231	.259								
−6.0	.010	.010	.012	.012	.021	.021	.022	.028	.041		
	.066	.170	.208								
−4.0	.010	.010	.009	.009	.009	.009	.008	.010	.011		
	.014	.118	.177								
−2.0	.008	.008	.008	.008	.008	.008	.007	.008	.008		
	.009	.097	.149								
0.0	.006	.006	.006	.006	.006	.006	.006	.006	.006		
	.013	.091	.149								
2.0	.006	.006	.006	.006	.006	.006	.007	.006	.008		
	.038	.128	.175								
4.0	.009	.009	.008	.008	.008	.008	.008	.007	.016		
	.067	.175	.218								
6.0	.010	.010	.010	.010	.010	.010	.011	.013	.035		
	.090	.215	.253								
8.0	.013	.013	.013	.013	.019	.013	.027	.044	.088		
	.168	.261	.299								
10.0	.017	.017	.036	.036	.060	.017	.056	.093	.138		
	.230	.305	.339								
12.0	.034	.034	.151	.151	.138	.034	.163	.143	.165		
	.268	.337	.367								
14.0	.240	.240	.235	.235	.226	.240	.197	.198	.266		
	.305	.370	.397								
16.0	.284	.284	.283	.283	.290	.290	.310	.320	.330		
	.343	.403	.428								
20.0	.320	.320	.320	.32	.332	.332	.356	.368	.384		
	.412	.464	.481								
24.0	.37	.37	.37	.37	.38	.38	.39	.40	.41		
	.45	.51	.53								
30.0	.46	.47	.49	.49	.50	.50	.55	.60	.64		
	.67	.68	.69								
45.0	1.1	1.1	1.1	1.1	1.1	1.1	1.1	1.1	1.1		
	1.2	1.3	1.4								
90.0	2.1	2.1	2.1	2.1	2.1	2.1	2.1	2.1	2.1		
	2.1	2.1	2.1								
180.	.017	.016	.015	.015	.014	.014	.013	.012	.011		
	.050	.11	.11								
	0.0	0.3	0.4	0.42	0.5	0.52	0.6	0.66	0.71		
	0.76	0.81	0.85								
−180.	−.14	−.14	−.14	−.135	−.13	−.12	−.12	−.12	−.12		
	−.12	−.11	−.10								
−90.	−.5	−.5	−.5	−.5	−.5	−.5	−.5	−.5	−.5		
	−.5	−.5	−.5								
−45.	.5	.5	.5	.5	.5	.5	.5	.5	.5		
	.5	.5	.5								
−10.	.045	.045	.047	.047	.057	.057	−.045	−.028	−.007		
	.048	.079	.26								
−8.	−.019	−.019	−.015	−.015	−.004	−.004	−.045	−.028	−.007		
	.048	.057	.209								
−6.	−.016	−.016	−.018	−.018	−.022	−.022	−.027	−.03	−.024		
	0.0	.035	.157								
−4.	−.016	−.016	−.017	−.017	−.018	−.018	−.02	−.021	−.024		
	.006	.002	.079								

```
-2.    -.017   -.017   -.017   -.017   -.019   -.019   -.02    -.021   -.021
       -.024   -.0196  .027
0.0    -.017   -.017   -.017   -.017   -.019   -.019   -.021   -.023   -.027
       -.034   -.025   -.025
2.0    -.018   -.018   -.019   -.019   -.021   -.02    -.024   -.027   -.027
       -.054   -.030   -.077
4.0    -.019   -.019   -.02    -.02    -.021   -.021   -.024   -.029   -.035
       -.071   -.052   -.13
6.0    -.018   -.018   -.019   -.019   -.019   -.019   -.017   -.020   -.039
       -.089   -.085   -.21
8.0    -.017   -.017   -.016   -.016   -.011   -.011   -.010   -.022   -.061
       -.089   -.107   -.259
10.    -.014   -.014   -.009   -.009   -.006   -.006   -.012   -.04    -.086
       -.107   -.129   -.31
12.    -.009   -.009   -.055   -.055   -.053   -.053   -.074   -.08    -.116
       -.133   -.151   -.363
14.    -.097   -.097   -.103   -.103   -.107   -.107   -.112   -.115   -.16
       -.159   -.173   -.410
16.    -.118   -.118   -.123   -.123   -.177   -.177   -.187   -.188   -.186
       -.186   -.184   -.440
20.    -.121   -.121   -.123   -.123   -.20    -.20    -.27    -.27    -.24
       -.23    -.23    -.5
24.    -.15    -.15    -.2     -.2     -.23    -.23    -.27    -.27    -.26
       -.25    -.25    -.5
30.    -.20    -.23    -.256   -.256   -.27    -.27    -.28    -.28    -.28
       -.27    -.28    -.5
45.    -.5     -.5     -.5     -.5     -.5     -.5     -.5     -.5     -.5
       -.5     -.5     -.5
90.    .5      .5      .5      .5      .5      .5      .5      .5      .5
       .5      .5      .5
180.   .09     .09     .087    .087    .085    .085    .08     .08     .072
       .066    .06     .05
```

CLCD3017 for XV–15, RLM 4/30/75, r = .7–.9

C81 table for the fourth blade segment (0.95–1.0 *R*):

```
64-X08 2-D   AERODYNAMICS     122312231223
       0.0     0.3     0.4     0.42    0.5     0.52    0.6     0.66    0.71
       0.76    0.81    0.85
-180.  -.15    -.15    -.15    -.15    -.15    -.15    -.15    -.15    -.15
       -.15    -.15    -.15
-90.   0.0     0.0     0.0     0.0     0.0     0.0     0.0     0.0     0.0
       0.0     0.0     0.0
-45.   -1.0    -1.0    -1.0    -1.0    -1.0    -1.0    -1.0    -1.0    -1.0
       -1.0    -1.0    -1.0
-10.   -.75    -.74    -.60    -.60    -.578   -.578   -.612   -.701   -.70
       -.60    -.55    -.45
-8.0   -.74    -.74    -.60    -.60    -.578   -.578   -.612   -.701   -.72
       -.70    -.60    -.50
-6.0   -.541   -.541   -.554   -.554   -.578   -.578   -.612   -.701   -.76
       -.771   -.68    -.575
-4.0   -.340   -.340   -.353   -.353   -.368   -.368   -.401   -.429   -.482
       -.547   -.44    -.435
-2.0   -.116   -.116   -.120   -.120   -.129   -.129   -.145   -.154   -.168
       -.193   -.121   -.115
```

0.0	.091	.091	.095	.095	.101	.101	.111	.118	.130
	.150	.217	.185						
2.0	.323	.323	.334	.334	.357	.357	.389	.416	.461
	.510	.510	.490						
4.0	.545	.545	.569	.569	.604	.604	.665	.712	.767
	.774	.765	.660						
6.0	.772	.772	.794	.794	.840	.840	.916	1.001	.987
	.956	.910	.740						
8.0	.950	.950	.937	.937	.981	.981	1.148	1.157	1.126
	1.08	.945	.780						
10.0	1.02	1.009	.994	.994	.995	.995	1.233	1.142	1.218
	1.13	.980	.780						
12.0	1.05	1.004	.986	.986	.960	.960	.965	.950	1.220
	1.14	1.0	.80						
14.0	1.0	.955	.982	.982	.995	.995	.900	.880	1.15
	1.15	1.03	.850						
16.0	.888	.888	1.0	1.0	1.06	1.06	.900	.870	1.00
	1.16	1.08	.90						
20.0	.968	.968	1.05	1.05	1.11	1.11	.980	.980	.93
	1.17	1.12	.980						
24.0	1.07	1.07	1.10	1.10	1.150	1.150	1.07	1.07	1.07
	1.17	1.15	1.07						
30.0	1.175	1.175	1.175	1.175	1.175	1.175	1.175	1.175	1.175
	1.175	1.175	1.175						
45.0	1.25	1.25	1.25	1.25	1.25	1.25	1.25	1.25	1.25
	1.25	1.25	1.25						
90.0	0.0	0.0	0.0	0.0	0.0	0.0	0.0	0.0	0.0
	0.0	0.0	0.0						
180.	.15	.15	.15	.15	.15	.15	.15	.15	.15
	.15	.15	.15						
	0.0	0.3	0.4	0.42	0.5	0.52	0.6	0.66	0.71
	0.76	0.81	0.85						
−180.	.024	.024	.023	.023	.02	.019	.018	.017	.017
	.017	.016	.012						
−90.	2.1	2.1	2.1	2.1	2.1	2.1	2.1	2.1	2.1
	2.1	2.1	2.1						
−45.	1.2	1.2	1.2	1.2	1.2	1.2	1.2	1.2	1.2
	1.2	1.2	1.2						
−10.	.106	.106	.118	.118	.154	.154	.174	.19	.204
	.233	.270	.33						
−8.	.04	.04	.05	.05	.08	.08	.08	.09	.10
	.15	.16	.20						
−6.	.016	.016	.023	.023	.060	.060	.057	.054	.075
	.102	.11	.12						
−4.	.009	.009	.009	.009	.016	.016	.019	.020	.026
	.044	.067	.104						
−2.	.007	.007	.007	.007	.008	.008	.008	.008	.009
	.010	.015	.049						
0.0	.005	.005	.005	.005	.006	.006	.006	.006	.006
	.006	.019	.049						
2.0	.005	.005	.005	.005	.005	.005	.005	.006	.006
	.016	.045	.095						
4.0	.008	.008	.007	.007	.008	.008	.008	.009	.011
	.037	.105	.147						
6.0	.009	.009	.010	.010	.013	.013	.019	.028	.049
	.062	.149	.186						
8.0	.015	.015	.052	.052	.056	.056	.061	.074	.098
	.155	.203	.236						

10.0	.134	.134	.137	.137	.143	.143	.144	.145	.153
	.214	.253	.287						
12.0	.223	.223	.215	.215	.22	.22	.24	.25	.26
	.266	.305	.337						
14.0	.282	.282	.247	.247	.25	.25	.26	.27	.28
	.319	.355	.387						
16.0	.253	.253	.255	.255	.27	.27	.28	.29	.30
	.33	.39	.40						
20.0	.270	.270	.280	.280	.30	.30	.32	.33	.34
	.35	.42	.45						
24.0	.29	.29	.30	.30	.32	.32	.36	.37	.38
	.39	.45	.47						
30.0	.32	.32	.33	.33	.35	.35	.38	.39	.40
	.55	.57	.65						
45.0	1.2	1.2	1.2	1.2	1.2	1.2	1.2	1.2	1.2
	1.2	1.2	1.2						
90.	2.1	2.1	2.1	2.1	2.1	2.1	2.1	2.1	2.1
	2.1	2.1	2.1						
180.	.024	.024	.023	.023	.020	.020	.019	.018	.017
	.017	.016	.012						
	0.0	0.3	0.4	0.42	0.5	0.52	0.6	0.66	0.71
	0.76	0.81	0.85						
−180.	−.15	−.15	−.15	−.15	−.15	−.15	−.145	−.14	−.13
	−.13	−.125	−.11						
−90.	−.5	−.5	−.5	−.5	−.5	−.5	−.5	−.5	−.5
	−.5	−.5	−.5						
−45.	.5	.5	.5	.5	.5	.5	.5	.5	.5
	.5	.5	.5						
−10.	−.02	−.02	−.02	−.02	−.02	−.02	0.	−.01	.031
	.04	.10	.22						
−8.	−.02	−.02	−.02	−.02	−.02	−.02	−.02	−.03	.001
	.016	.10	.168						
−6.	−.021	−.021	−.018	−.018	−.016	−.016	−.022	−.041	−.029
	0.	0.1	0.142						
−4.	−.02	−.02	−.021	−.021	−.024	−.024	−.029	−.034	−.038
	−.027	−.1	0.06						
−2.	−.019	−.019	−.02	−.02	−.022	−.022	−.024	−.026	−.028
	−.034	−.016	.012						
0.0	−.02	−.02	−.02	−.02	−.022	−.022	−.024	−.026	−.028
	−.04	−.083	−.10						
2.0	−.02	−.02	−.021	−.021	−.023	−.023	−.025	−.027	−.029
	−.051	−.159	−.159						
4.0	−.019	−.019	−.021	−.021	−.022	−.022	−.024	−.025	−.03
	−.084	−.159	−.159						
6.0	−.019	−.019	−.018	−.018	−.017	−.017	−.012	−.015	−.045
	−.123	−.159	−.19						
8.0	−.014	−.014	−.012	−.012	−.013	−.013	−.001	−.02	−.077
	−.123	−.159	−.24						
10.	−.042	−.042	−.055	−.055	−.064	−.064	−.069	−.037	−.097
	−.123	−.133	−.30						
12.	−.10	−.10	−.106	−.106	−.110	−.110	−.110	−.111	−.14
	−.148	−.155	−.352						
14.	−.126	−.126	−.11	−.11	−.113	−.113	−.16	−.16	−.17
	−.174	−.177	−.404						
16.	−.121	−.121	−.11	−.11	−.19	−.19	−.20	−.20	−.203
	−.201	−.20	−.45						
20.	−.15	−.15	−.15	−.15	−.20	−.20	−.23	−.23	−.23
	−.23	−.23	−.5						

```
24.    -.17    -.17    -.17    -.17    -.25    -.25    -.25    -.25    -.25
       -.25    -.25    -.5
30.    -.25    -.25    -.27    -.27    -.29    -.29    -.30    -.30    -.30
       -.29    -.29    -.5
45.    -.5     -.5     -.5     -.5     -.5     -.5     -.5     -.5     -.5
       -.5     -.5     -.5
90.    .5      .5      .5      .5      .5      .5      .5      .5      .5
       .5      .5      .5
180.   .07     .07     .07     .07     .068    .068    .065    .06     .057
       .051    .044    .03
```

CLCD3018 for XV-15, RLM 4/30/75, r = .9-1.0

Appendix B

0.15-*t/c* Wing Design

To evaluate proprotor design options for improving whirl-flutter stability, a notional XV-15 with a 0.15-*t/c* graphite-epoxy wing was conceptually defined. The wing characteristics were estimated using the methods presented in reference 21. These methods are appropriate for estimating tiltrotor wing strength, stiffness, and weight at a conceptual design level.

The wing is assumed to have the same geometry as the XV-15 wing except for reduced thickness. The structural concept is a constant cross-section, uniform-wall-thickness, single-cell torque box. Figure B1 compares the 0.15- and 0.23-*t/c* wing sections. It also shows the torque-box geometry assumed in the design. The torque box reacts beam bending, chord bending, shear, and torsion loads. Upper and lower spar caps provide additional beam bending strength. The spar caps are assumed concentrated at the maximum wing thickness.

The primary structure is assumed to be T300/5208 graphite epoxy. The torque-box skin is a balanced and symmetric laminate with 30% 0-deg plies, 65% ±45-deg plies, and 5% 90-deg plies. The wing-spar caps are 85% 0-deg plies and 15% 90-deg plies. This simple model does not include structural coupling from the use of tailored (unbalanced) torque-box skins (investigations in composite tailoring of the torque-box structure to improve tiltrotor whirl-mode stability are described in references 2, 3, and 5).

The wing structure is sized based on static strength to meet 2-g jump takeoff with the nacelles positioned at 90 deg (helicopter mode) and 4-g pull-up with the nacelles at 0 deg (airplane mode). The wing is calculated to have a static torsional divergence speed of 529 knots at sea-level standard conditions. The wing structure is not sized to meet a minimum whirl-flutter speed requirement.

The design characteristics of the 0.15-*t/c* wing are compared with the original XV-15 in table B1; see also table 1 in the main body of this report.
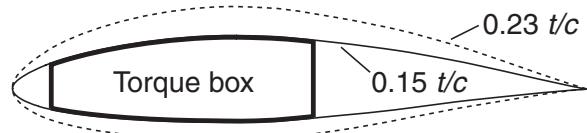

*Figure B1. 0.23- and 0.15-*t/c *wing sections, with the torque box highlighted for the thinner section.*

TABLE B1. WING STRUCTURAL COMPARISON.

	XV-15 wing (0.23 *t/c*)	Conceptual wing (0.15 *t/c*)
Weights:		
Torque box, lb	567	260
Spars, lb	52	34
Control surfaces, lb	97	77
Fairings, lb	108	86
Fittings, other, lb	122	122
Total wing, lb	946	579
Material Properties:		
Material	Aluminum	Graphite epoxy
Elastic modulus, torque box, lb/in^2	10,000,000	9,000,000
Elastic modulus, spars, lb/in^2	10,000,000	18,000,000
Shear Modulus, torque box, lb/in^2	3,800,000	3,750,000
Density, lb/in^3	0.10	0.06
Limit strain, in/in	0.0068	0.0047

Appendix C

XV-15 Tiltrotor Finite-Element Stick Model

Introduction

This appendix describes the tiltrotor finite-element stick models used in the aeroelastic stability predictions presented in this paper. The models are based on the Bell XV-15 tiltrotor structural characteristics. The "thick-wing" model consists of an elastic wing with 0.23 *t/c*. The model uses one-dimensional elements exclusively, hence the name "stick" model. The normal modes of this stick model were calculated using MSC NASTRAN for Windows (ref. 17). A CAMRAD II (ref. 14) aeroelastic-stability analysis was performed using the stick-model mode shapes, frequencies, and modal masses as input data. The stick-model CAMRAD II stability results were compared with CAMRAD II stability results using frequencies and mode shapes from a detailed NASTRAN structural model of the XV-15 (ref. 22). There was good agreement between the CAMRAD II stick-model aeroelastic-stability results and the CAMRAD II detailed NASTRAN model aeroelastic-stability results.

The stick-model structural properties were revised to represent an XV-15 tiltrotor with a 0.15-*t/c* composite wing. The mode shapes, frequencies, and modal masses of this model were used to create a CAMRAD II aeroelastic stability model of the XV-15 with a 0.15-*t/c* wing. This "thin-wing" CAMRAD II model was used to assess the effect of proprotor design parameters on aeroelastic stability as presented in the body of this report.

Finite-Element Stick-Model Development

The finite-element stick model was developed using the XV-15 finite-element stick model by Wolkovitch et al. (ref. 23) as a starting point. The model is based on the XV-15 geometry (fig. 2), weights (ref. 23), and wing structural characteristics (ref. 22). The model consists of a 10-element elastic wing with a rigid fuselage and rigid wing-tip mounted nacelles (fig. C1). Two concentrated masses model the left and right rotors and hubs. The following are additions to the Wolkovitch model to more closely model the actual XV-15 airframe structural characteristics:

1. The wing is assumed rigid in torsion and chord bending between the wing-to-fuselage mounting points at butt lines of 28 and –28 inches (the wing is assumed elastic in beam bending between the wing-to-fuselage mounting points). This is done to account for the high stiffness at the mounting points created by the fuselage structure.

2. The fuselage and nacelle elements are offset below the plane of the wing. This lowers the fuselage and nacelle CGs relative to the wing. The fuselage and nacelle node points remain in the plane of the wing, the same as for the Wolkovitch model.

3. A roll-inertia element is added to the fuselage. The inertia of this element is adjusted to lower the wing antisymmetric beam-bending-mode frequency to match the detailed NASTRAN model antisymmetric beam-bending frequency.

The thick-wing stick-model characteristics are summarized in table C1. The stick-model geometry is compared with the XV-15 detailed NASTRAN geometry in figures C1 and C2. The NASTRAN inputs are listed in appendix D.

TABLE C1. XV-15 FINITE-ELEMENT STICK-MODEL CHARACTERISTICS.

Component	Element type	Number of elements	Length, ft	Weight, lb
Wing[a]	Elastic beam	10	32.4	2,534
Left and right nacelle	Rigid beam	4	7.7	3,166
Left and right rotor	Concentrated mass	2	0	1,118
Fuselage[b]	Rigid beam	2	42.1	6,182
	Concentrated roll inertia (4,833 slug-ft^2)	1	0	0
a. Includes fuel, cross shafting, etc.			Gross weight:	13,000
b. Includes equipment, crew, and payload				
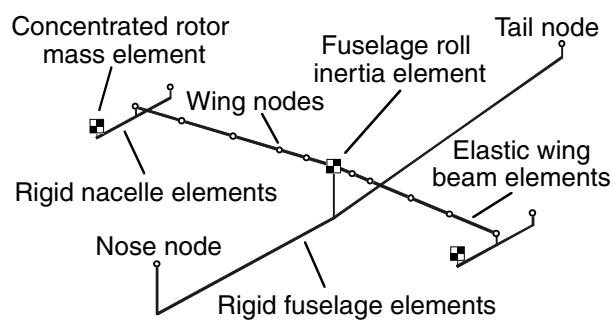
Figure C1. XV-15 finite-element stick model.
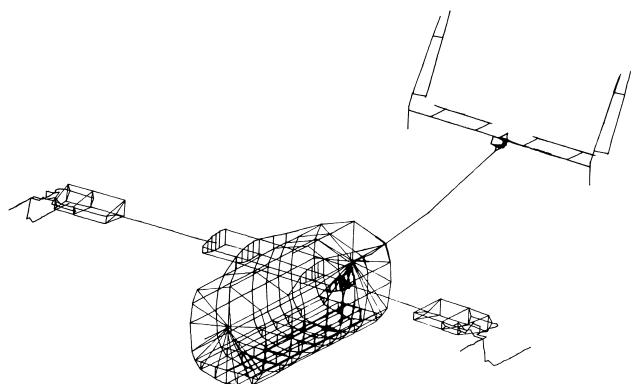
Figure C2. XV-15 detailed finite-element model (ref. 22).
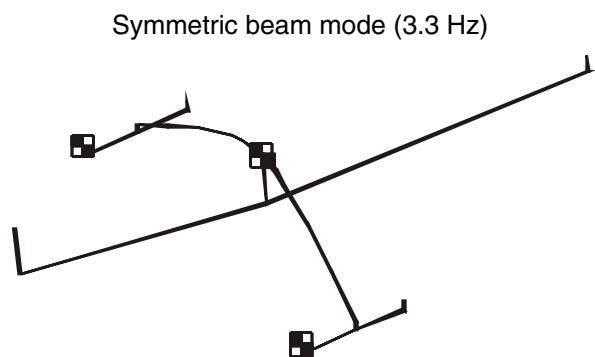
Symmetric beam mode (3.3 Hz)
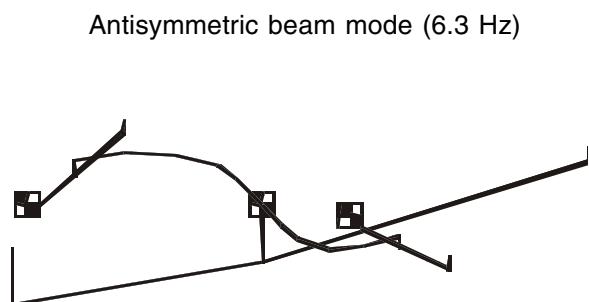
Antisymmetric beam mode (6.3 Hz)
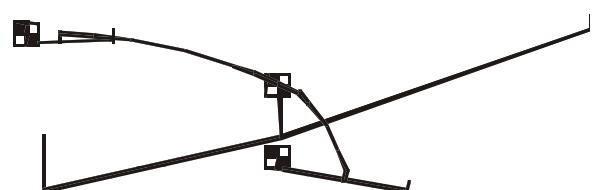
Symmetric chord mode (6.3 Hz)
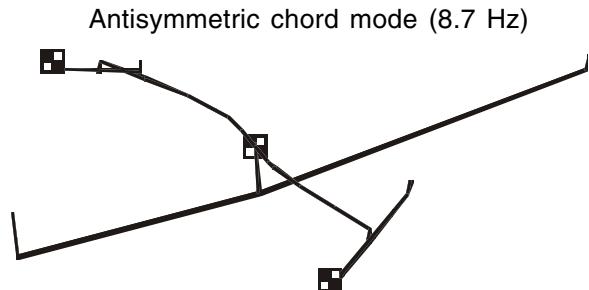
Antisymmetric chord mode (8.7 Hz)
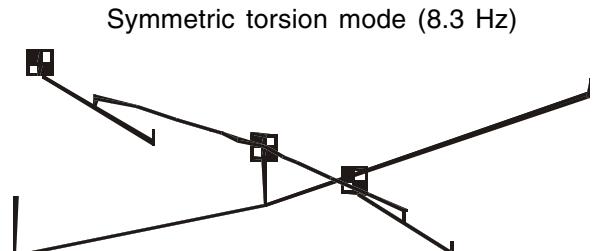
Symmetric torsion mode (8.3 Hz)
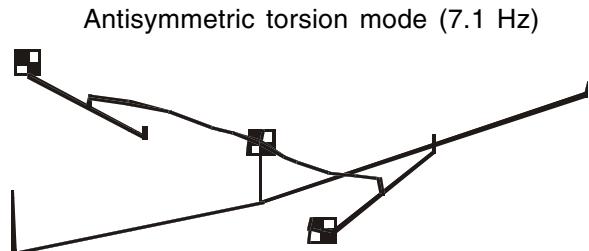

Antisymmetric torsion mode (7.1 Hz)

Figure C3. XV-15 stick-model mode shapes and frequencies (0.23 t/c wing).

Zero-Airspeed Mode Shapes and Frequencies

The six lowest-frequency airframe modes were calculated by NASTRAN for Windows and input into CAMRAD II. These modes correspond to three symmetric wing modes and three antisymmetric wing modes and are critical for whirl flutter. The mode shapes calculated by NASTRAN are shown in figure C3. Notice that the airframe mode shapes are highly coupled and hence the mode titles are somewhat arbitrary. For example, the antisymmetric beam mode has a large component of wing torsion as well as beam bending.

Tables C2–C4 present the modal data for the NASTRAN models used in this study. The mode frequency, mass, displacements, and rotations at the right rotor hub are shown for the stick model in table C2. The corresponding detailed NASTRAN model data are shown in table C3, and the data for the 0.15-t/c wing are shown in table C4. The structural damping given in table C2 is the same for all NASTRAN models.

Stick-Model Stability Results

The CAMRAD II aeroelastic stability analysis was performed with limited-power trim criteria (level flight up to maximum power, constant power thereafter). The rotor was trimmed to 458 rpm at sea-level standard conditions. The CAMRAD II stability results using the stick-model airframe modes for the thick wing are plotted in figures C4 and C5. For comparison, stability results using the detailed NASTRAN airframe model modes are also plotted in figures C4 and C5. The stick-model results are very similar to the detailed-model

results. The frequency and damping curves demonstrate similar characteristics.

CAMRAD II predicts a 24-knot higher symmetric chord-mode instability speed for the stick model than for the detailed model. The stick model yields an 11-knot higher antisymmetric beam-mode instability speed than the detailed model. The stick-model frequencies closely match those of the detailed model except for the antisymmetric chord mode and antisymmetric torsion modes. For example, the stick model overpredicts the antisymmetric chord-mode frequency by 0.4 Hz and underpredicts the antisymmetric torsion-mode frequency by 1.1 Hz compared to the detailed model at 300 knots airspeed. The results indicate that the simple finite-element stick model can be a useful substitute for a detailed finite-element model for predicting the aeroelastic stability of low-frequency airframe modes.

Stability of Stick Model with 0.15-t/c Wing

The 0.15-t/c wing stiffness and mass characteristics were input into the MSC NASTRAN for Windows XV-15 stick model. The mode frequencies and shapes of the 0.15-t/c wing model are listed in table C4. CAMRAD II stability predictions for the XV-15 with the 0.15-t/c wing are shown in figures 4 and 5 (the "thin-wing" predictions). The aeroelastic instability speed is reduced from 335 knots (antisymmetric beam mode) for the XV-15 with 0.23-t/c wing to 275 knots (antisymmetric beam mode) for the XV-15 with the conceptual 0.15-t/c wing. The CAMRAD II model of the XV-15 with 0.15-t/c wing serves as the baseline for evaluating proprotor design options for improving whirl-flutter stability, as presented in the main report.

TABLE C2. MODE SHAPES AT RIGHT HUB FOR XV-15 FINITE-ELEMENT STICK MODEL
(0.23-*t/c* WING).

Mode	Symmetric beam	Symmetric chord	Symmetric torsion	Antisymmetric beam	Antisymmetric chord	Antisymmetric torsion
Frequency, Hz	3.3	6.3	8.3	6.3	8.7	7.1
Modal mass, slugs	201.6	320.0	50.1	231.6	57.8	243.0
Structural damping	0.03	0.07	0.08	0.05	0.05	0.06
Displacement, ft						
X	−0.0275	1.0000	−0.1840	0.2702	−0.2500	0.7077
Y	0.0642	−0.9283	0.1235	−0.3044	0.0802	−0.3986
Z	1.0000	−0.2755	−0.5525	0.9438	−0.4516	−0.5767
Rotation, rad						
X	0.1385	0.0322	0.0405	0.1000	0.0651	0.0212
Y	−0.0251	0.1125	0.2027	−0.1561	0.1895	0.1951
Z	0.0025	−0.1903	0.0219	−0.0304	0.0308	−0.1244

TABLE C3. MODE SHAPES AT RIGHT HUB FOR XV-15 DETAILED FINITE-ELEMENT MODEL
(0.23-*t/c* WING).

Mode	Symmetric beam	Symmetric chord	Symmetric torsion	Antisymmetric beam	Antisymmetric chord	Antisymmetric torsion
Frequency, Hz	3.4	6.6	8.2	6.3	7.9	7.7
Modal mass, slugs	241.6	517.8	7.6	242.7	407.3	113.0
Displacement, ft						
X	−0.0014	−1.0000	−0.1142	−0.1329	−0.7699	−0.0763
Y	−0.0330	1.0311	0.0992	0.5231	0.3645	−0.1035
Z	−1.0000	1.1197	−0.2413	−0.8419	−0.5238	−0.9917
Rotation, rad						
X	−0.1463	−0.0698	0.0056	−0.1777	0.1012	0.0564
Y	0.0281	−0.3719	0.0800	0.1648	0.1914	0.3356
Z	0.0022	0.2615	0.0263	0.0384	0.1780	−0.0227

TABLE C4. MODE SHAPES AT RIGHT HUB FOR TILTROTOR WITH CONCEPTUAL
0.15-*t/c* WING.

| Mode	Symmetric beam	Symmetric chord	Symmetric torsion	Antisymmetric beam	Antisymmetric chord	Antisymmetric torsion
Frequency, Hz	2.4	5.1	6.0	4.6	6.5	5.5
Modal mass, slugs	194.8	154.6	66.5	199.1	117.1	86.6
Displacement, ft						
X	−0.0247	0.5407	−0.3597	0.1529	0.5504	−0.2675
Y	0.0620	−0.5340	0.2820	−0.2239	−0.2319	0.2010
Z	1.0000	−0.5074	−0.5447	1.0000	0.4176	0.4311
Rotation, rad						
X	0.1362	0.0481	0.0407	0.0796	−0.0754	−0.0594
Y	−0.0289	0.1968	0.2017	−0.1953	−0.1851	−0.1869
Z	0.0022	−0.1117	0.0540	−0.0095	−0.0791	0.0522
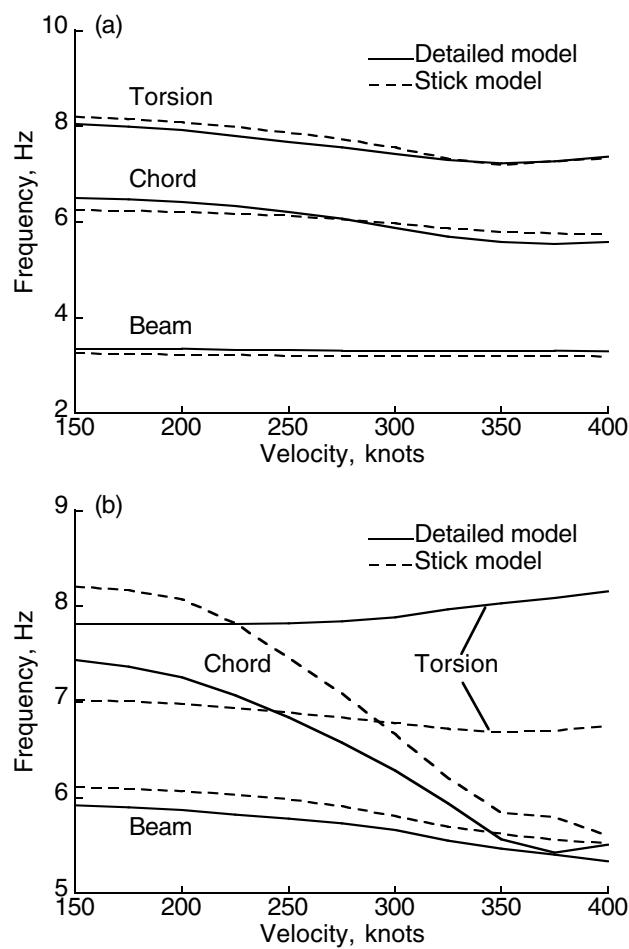
Figure C4. Frequency versus flight speed for XV-15 wing modes; (a) symmetric; (b) antisymmetric.
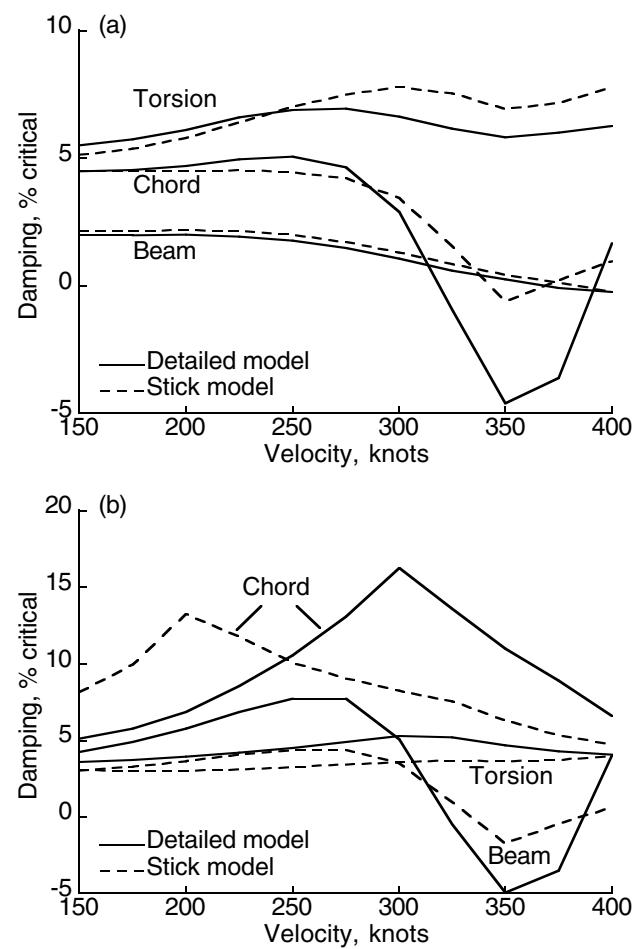

Figure C5. Damping versus flight speed for XV-15 wing modes; (a) symmetric; (b) antisymmetric.

Appendix D

The NASTRAN Model of the 0.15-*t/c* Wing

```
INIT MASTER(S)
ID M:\NASTR,MSC/N
SOL SEMODES
TIME 10000
DIAG 5
CEND
METHOD = 1
  ECHO = NONE
  DISPLACEMENT = ALL
  OLOAD = NONE
  SPCFORCE = NONE
  FORCE = NONE
  STRESS = NONE
BEGIN BULK
$ ************************************************************************
$   Written by : MSC/NASTRAN for Windows
$   Version    : 5.00
$   Translator : MSC/NASTRAN
$   From Model : M:\NASTRAN\15%WING\15%WING.MOD
$   Date       : Fri Dec 04 15:27:07 1998
$   Output To  : M:\NASTRAN\15%WING\15%WI002
$ ************************************************************************
$
PARAM,PRGPST,NO
PARAM,AUTOSPC,YES
PARAM,K6ROT,100.
PARAM,MAXRATIO,1.E+8
PARAM,GRDPNT,0
EIGRL          1      2.     10.      6       0                     MAX
CORD2C         1       0     0.      0.      0.      0.      0.      1.+MSC/NC1
+MSC/NC1     1.      0.      1.
CORD2S         2       0     0.      0.      0.      0.      0.      1.+MSC/NC2
+MSC/NC2     1.      0.      1.
$ Note:  Create mode shape output in CAMRAD coordinates.
$ MSC/NASTRAN for Windows Coordinate System 3 : CAMRAD 2
CORD2R         3       0     0.      0.      0.      0.      0.     -1.+CS     3
+CS    3    -1.      0.      0.
$ MSC/NASTRAN for Windows Property 2 : nacelle
PBEAM          2       2     1.      1.      1.      0.      1.      0.+PR     2
+PR    2     0.      0.      0.      0.      0.      0.      0.      0.+PA     2
+PA    2    YESA     1.                                              +PC      2
+PC    2     0.      0.
$ MSC/NASTRAN for Windows Property 4 : body
PBEAM          4       4     1.      1.      1.      0.      1.      0.+PR     4
+PR    4     0.      0.      0.      0.      0.      0.      0.      0.+PA     4
+PA    4    YESA     1.                                              +PC      4
+PC    4     0.      0.
$ MSC/NASTRAN for Windows Property 6 : wing1
$ Note: The wing is assumed to be rigid in the axial direction
$
PBEAM          6       6 1.E+131.982E+97.589E+9      0.1.331E+9 0.0215+PR     6
+PR    6     0.      0.      0.      0.      0.      0.      0.      0.+PA     6
+PA    6    YESA     1.                                              +PC      6
+PC    6     0.      0.
```

43

```
$ MSC/NASTRAN for Windows Property 7 : wing2
PBEAM          7       7 1.E+131.982E+97.589E+9       0.1.331E+9 0.02002+PR     7
+PR     7      0.      0.      0.      0.      0.      0.      0.      0.+PA     7
+PA     7   YESA       1.                                              +PC     7
+PC     7      0.      0.
$ MSC/NASTRAN for Windows Property 8 : wing3
PBEAM          8       8 1.E+131.982E+97.589E+9       0.1.331E+9 0.01298+PR     8
+PR     8      0.      0.      0.      0.      0.      0.      0.      0.+PA     8
+PA     8   YESA       1.                                              +PC     8
+PC     8      0.      0.
$ MSC/NASTRAN for Windows Property 9 : wing4
PBEAM          9       9 1.E+131.982E+97.589E+9       0.1.331E+90.003149+PR     9
+PR     9      0.      0.      0.      0.      0.      0.      0.      0.+PA     9
+PA     9   YESA       1.                                              +PC     9
+PC     9      0.      0.
$ MSC/NASTRAN for Windows Property 11 : wing mount
PBEAM         11       6 1.E+131.982E+9  1.E+13       0.  1.E+130.021497+PR     B
+PR     B      0.      0.      0.      0.      0.      0.      0.      0.+PA     B
+PA     B   YESA       1.                                              +PC     B
+PC     B      0.      0.
$ MSC/NASTRAN for Windows Material 2 : nacelle
MAT1           2  1.E+13  1.E+13          0.044638      0.      0.
$ MSC/NASTRAN for Windows Material 4 : body
MAT1           4  1.E+13  1.E+13          0.031801      0.      0.
$ MSC/NASTRAN for Windows Material 6 : wing1
MAT1           6      1.      1.                0.      0.      0.
$ MSC/NASTRAN for Windows Material 7 : wing2
MAT1           7      1.      1.                0.      0.      0.
$ MSC/NASTRAN for Windows Material 8 : wing3
MAT1           8      1.      1.                0.      0.      0.
$ MSC/NASTRAN for Windows Material 9 : wing4
MAT1           9      1.      1.                0.      0.      0.
$ Right wing tip
GRID           1       0 288.68    193.    6.74       3
$ Right wing
GRID           2       0 294.178 144.75    5.05       3
$ Right wing
GRID           3       0 299.675   96.5    3.37       3
$ Right wing
GRID           4       0 305.173  48.25   1.684       3
$ Center wing
GRID           5       0 310.67      0.      0.       3
$ Left wing
GRID           6       0 305.173 -48.25   1.684       3
$ Left wing
GRID           7       0 299.675  -96.5    3.37       3
$ Left wing
GRID           8       0 294.178 -144.75   5.05       3
$ Left wing
GRID           9       0 288.68   -193.    6.74       3
$ Right proprotor hub
GRID          10       0 241.38    193.    6.74       3
$ Left proprotor hub
GRID          11       0 241.38   -193.    6.74       3
$ Right aft nacelle
GRID          12       0 333.29    193.    6.74       3
$ Left aft nacelle
GRID          13       0 333.29   -193.    6.74       3
```

```
$ Body nose
GRID           14       0  92.525       0.       0.       3
$ Body tail
GRID           15       0  597.52       0.       0.       3
$ Right wing mount
GRID           16       0 307.921      28.    0.977       3
$ Left wing mount
GRID           17       0 307.921     -28.    0.977       3
CBEAM           1       9       1       2       0.       0.      -1.
CBEAM           2       8       2       3       0.       0.      -1.
CBEAM           3       7       3       4       0.       0.      -1.
CBEAM           4       6       4      16       0.       0.      -1.
CBEAM           5      11       5      17       0.       0.      -1.
CBEAM           6       7       6       7       0.       0.      -1.
CBEAM           7       8       7       8       0.       0.      -1.
CBEAM           8       9       8       9       0.       0.      -1.
CBEAM           9       2      10       1       0.       0.      -1.       +EL       9
+EL     9                       0.       0.       9.       0.       0.       9.
CBEAM          10       2       1      12       0.       0.      -1.       +EL       A
+EL     A                       0.       .0       9.       0.       0.       9.
CBEAM          11       2      11       9       0.       0.      -1.       +EL       B
+EL     B                       0.       .0       9.       0.       0.       9.
CBEAM          12       2       9      13       0.       0.      -1.       +EL       C
+EL     C                       0.       .0       9.       0.       0.       9.
$ Right proprotor point mass
CONM2          13      10       0 1.44599       0.       0.       0.       +EL       D
+EL     D      0.      0.      0.      0.       0.       0.
$ Left proprotor point mass
CONM2          14      11       0 1.44599       0.       0.       0.       +EL       E
+EL     E      0.      0.      0.      0.       0.       0.
CBEAM          15       4      14       5       0.       0.      -1.       +EL       F
+EL     F                       0.       0.     43.2       0.       0.     43.2
CBEAM          16       4       5      15       0.       0.      -1.       +EL       G
+EL     G                       0.       0.     43.2       0.       0.      11.
$ Fuselage roll inertia
CONM2          17       5       0       0.       0.       0.       0.       +EL       H
+EL     H  58000.      0.      0.      0.       0.       0.
CBEAM          18      11      16       5       0.       0.      -1.
CBEAM          19       6      17       6       0.       0.      -1.
ENDDATA
```

Appendix E

Limitations of the Analysis

The CAMRAD II model of the XV-15 used for the research reported here has several known deficiencies. Most significant is the rotor model, which was derived from an older model developed for an earlier version of CAMRAD (essentially that of ref. 24). That model was based on preproduction blade data. Although conversion to CAMRAD II automatically provided some improvements, especially in the analysis of blade dynamics, numerous deficiencies remain:

1. The radial stations are more sparsely distributed than is desirable for modeling sweep.

2. The control-system kinematics do not properly model the XV-15 collective/cyclic mixer ("spider") above the rotor, but instead assume a conventional swashplate below the rotor.

3. The airframe aerodynamics are only approximate.

4. The beam elements in the blade model are not optimally specified for modeling sweep.

Several cases were run to evaluate the adequacy of the model within these limitations. By far the largest differences occurred at 400 knots, well beyond the stability boundary, or for the antisymmetric wing chord mode, which was extremely stable. The following discussion is limited to the unstable modes within the stability boundary.

Trim Model Checks

It has previously been mentioned that the trim model was not the same for all cases, but was consistent within groups of cases. For trim, blade deflections were calculated using six rigid and nine flexible degrees of freedom (ref. 16). To check the adequacy of these calculations, a speed sweep of the baseline XV-15 was run with a modal analysis of blade deflections in trim; the model was otherwise the same as that used to generate the baseline predictions of figures C4 and C5 (the "detailed-model" predictions). This analysis used six blade modes, up to about 9.8/rev, and six harmonics, the same as used for the loads calculations in figures 27 and 28. The results had a maximum change of +0.18% critical damping below the stability boundary, in this case for the symmetric wing chord mode.

For both trim models (those using static and modal blade deflections), the trim tolerance was decreased by a factor of five. The maximum change in predicted damping below the stability boundary was –0.17% critical damping for the antisymmetric wing beam-bending mode.

Blade Model Checks

To check the adequacy of the blade beam-element model, the number of elements outboard of the pitch bearing was doubled from three to six elements. The results had a maximum change of +0.56% critical damping below the stability boundary for the antisymmetric wing beam-bending mode.

Flutter Model Checks

To check the adequacy of the flutter model, the number of blade modes used in the flutter calculations was doubled from four to eight per blade (about 16.1/rev). The maximum changes below the stability boundary were +0.11% critical damping for symmetric wing chord mode and –0.11% for the antisymmetric wing beam-bending mode.

Taken together, these checks of the model show that the options used for trim and flutter calculations were adequate for the purposes of the present research. The most promising area of improvement is in the number and distribution of the beam elements in the blade model.

Model Developments

As of this writing, an entirely new CAMRAD II model of the XV-15 is under development. It is based on production blade data, with better radial resolution. The control-system model has an overhead swashplate to better represent the spider. The new model includes the airframe aerodynamics tables of reference 25, for a much better match to flight trim data. The blade beam-element model is also improved.

More accurate predictions of airframe modes, hence aeroelastic stability, could obviously be achieved with a more sophisticated NASTRAN model. However, it is the trend of stability with airspeed that is crucial for the present research, and the stick model captures the modal trends reasonably well.

REPORT DOCUMENTATION PAGE

Form Approved
OMB No. 0704-0188

Public reporting burden for this collection of information is estimated to average 1 hour per response, including the time for reviewing instructions, searching existing data sources, gathering and maintaining the data needed, and completing and reviewing the collection of information. Send comments regarding this burden estimate or any other aspect of this collection of information, including suggestions for reducing this burden, to Washington Headquarters Services, Directorate for information Operations and Reports, 1215 Jefferson Davis Highway, Suite 1204, Arlington, VA 22202-4302, and to the Office of Management and Budget, Paperwork Reduction Project (0704-0188), Washington, DC 20503.

1. AGENCY USE ONLY *(Leave blank)*	2. REPORT DATE March 2004	3. REPORT TYPE AND DATES COVERED Technical Publication – September 1998-June 2001

4. TITLE AND SUBTITLE

Rotor Design Options for Improving XV-15 Whirl-Flutter Stability Margins

5. FUNDING NUMBERS

21-745

6. AUTHOR(S)

C. W. Acree, Jr.[1], R. J. Peyran[2], and W. Johnson[1]

7. PERFORMING ORGANIZATION NAME(S) AND ADDRESS(ES)

[1]Ames Research Center, Moffett Field, CA 94035-1000

[2]Aeroflightdynamics Directorate, U.S. Army Research, Development, and Engineering Command, Ames Research Center, Moffett Field, CA 94035-1000

8. PERFORMING ORGANIZATION REPORT NUMBER

A-0309307

9. SPONSORING/MONITORING AGENCY NAME(S) AND ADDRESS(ES)

National Aeronautics and Space Administration
Washington, DC 20546-0001

U.S. Army Research, Development, and Engineering Command
5183 Blackhawk Rd., Aberdeen Proving Ground, MD 21010-5424

10. SPONSORING/MONITORING AGENCY REPORT NUMBER

NASA/TP–2004-212262
AFDD/TR-04-001

11. SUPPLEMENTARY NOTES

Point of Contact: C. W. Acree, Ames Research Center, MS T12-B, Moffett Field, CA 94035-1000
(650) 604-5423

12a. DISTRIBUTION/AVAILABILITY STATEMENT

Unclassified — Unlimited
Subject Category 09   Distribution: Standard
Availability: NASA CASI (301) 621-0390

12b. DISTRIBUTION CODE

13. ABSTRACT *(Maximum 200 words)*

Rotor design changes intended to improve tiltrotor whirl-flutter stability margins were analyzed. A baseline analytical model of the XV-15 was established, and then a thinner, composite wing was designed to be representative of a high-speed tiltrotor. The rotor blade design was modified to increase the stability speed margin for the thin-wing design. Small rearward offsets of the aerodynamic-center locus with respect to the blade elastic axis created large increases in the stability boundary. The effect was strongest for offsets at the outboard part of the blade, where an offset of the aerodynamic center by 10% of tip chord improved the stability margin by over 100 knots. Forward offsets of the blade center of gravity had similar but less pronounced effects. Equivalent results were seen for swept-tip blades. Appropriate combinations of sweep and pitch stiffness completely eliminated whirl flutter within the speed range examined; alternatively, they allowed large increases in pitch-flap coupling (delta-three) for a given stability margin. A limited investigation of the rotor loads in helicopter and airplane configuration showed only minor increases in loads.

14. SUBJECT TERMS

XV-15, tiltrotor, whirl flutter, aeroelastic stability

15. NUMBER OF PAGES

52

16. PRICE CODE

17. SECURITY CLASSIFICATION OF REPORT Unclassified	18. SECURITY CLASSIFICATION OF THIS PAGE Unclassified	19. SECURITY CLASSIFICATION OF ABSTRACT Unclassified	20. LIMITATION OF ABSTRACT Unclassified